Dissolved iron in the Arctic shelf seas and surface waters of the Central Arctic Ocean: Impact of Arctic river water and ice-melt.

M.B. Klunder, D. Bauch, P. Laan, H.J.W. De Baar, S. van Heuven, S. Ober

Abstract:

Concentrations of dissolved (<0.2 μm) Fe (DFe) in the Arctic shelf seas and in the surface waters of the Central Arctic Ocean are presented. In the Barents and Kara seas, near-surface DFe minima indicate depletion of DFe by phytoplankton growth. Below the surface, lower DFe concentrations in the Kara Sea (~0.4-0.6 nM) than in the Barents Sea (~0.6-0.8 nM) likely reflect scavenging removal or biological depletion of DFe. Very high DFe concentrations (>10 nM) in the bottom waters of the Laptev Sea shelf may be attributed to either sediment resuspension, sinking of brine or regeneration of DFe in the lower layers. A significant correlation ($R^2 = 0.60$) between salinity and DFe is observed. Using $\delta^{18}O$, salinity ,nutrients and total alkalinity data, the main source for the high (>2 nM) DFe concentrations in the Amundsen and Makarov Basins is identified as (Eurasian) river water, transported with the Transpolar Drift (TPD). On the North American side of the TPD, the DFe concentrations are low (< 0.8 nM) and variations are determined by the effects of sea-ice meltwater, biological depletion and remineralization and scavenging in halocline waters from the shelf. This distribution pattern of DFe is also supported by the ratio between unfiltered and dissolved Fe (high (> 4) above the shelf and low (< 4) off the shelf).

1. Introduction

The Arctic Ocean is linked to the global thermohaline circulation, mainly through a strong contribution of Arctic Ocean waters to North Atlantic Deep Water [*Rudels*, 2001]. Due to ice cover and harsh conditions, the Arctic Ocean is one of the least studied oceans, and knowledge of the trace metal distributions of the Arctic Ocean is very limited. In contrast to other world Oceans, the Arctic Ocean is characterized by vast continental shelves (over 1/3 of the total Arctic Ocean area) and by a strong (seasonal) input of fresh water to surface waters from Siberian rivers (Ob, Yenisey, Lena) and North American rivers (Mackenzie) and by seasonal ice-melt [*Aagaard et al.*, 1981]. This freshwater causes a strong density difference between the mixed layer and deeper waters, which limits winter convection [*Rudels,* 2001]. These physical circumstances are expected to affect the distribution of dissolved iron (DFe) in the water column of the Arctic, resulting in a deviation from the vertical distribution common to open ocean profiles [*Johnson et al.*, 1997; *Moore and Braucher*, 2008]. Instead, in the Arctic Ocean, the strong lateral DFe supply into the stratified surface layers and relatively little vertical mixing are expected to result in high DFe concentrations in the surface layers, relative to lower concentrations at depth.

In other regions in the global ocean, Fe availability has been shown to be of vital importance to phytoplankton growth [*Martin and Gordon*, 1988; *de Baar et al.*, 1995; *Boyd et al.*, 2000]. In the Arctic, despite low temperatures and relatively low light levels, significant primary production is reported, most notably on the vast Arctic shelves [*Carmack and Wassmann,*2006; *Arrigo et al.*, 2008]. Recently more has become known about the role of light, temperature and nutrients in primary production in the Arctic Ocean [*Gosselin et al.*, 1997; *Pabi et al.*, 2008]. However, little is still known about the distribution of DFe and the role of DFe in Arctic primary production. A study by *Measures* [1999] showed reactive (unfiltered) Fe concentrations in the 1-4 nM range in the upper mixed layer over the central Arctic Ocean. They attributed these relatively high concentrations to melting of sea-ice with

entrained sediments. Indeed, *Nürnberg et al.* [1994] have shown the importance of sediment entrainment in sea-ice for transport of sediment from Arctic rivers to the Central Arctic Ocean. Therefore the mechanism of melting of sediment laden sea-ice is a possible DFe source to the Central Arctic. Mass balance models using $\delta^{18}O$, salinity and nutrients showed that fluvial input sources significantly affect the surface waters of the Central Arctic, which comprises about 5-15% river water [*Bauch et al.*, 1995; *Ekwurzel et al.*, 2001]. Model calculations indicate that river water in the Eurasian Basin is of Siberian origin [*Harms et al.*, 2000]. Moreover, based on Ba concentrations from the same cruise as ours, *Roeske et al.* [subm. man.] conclude that the observed river water is of Eurasian origin. Because DFe in the Siberian rivers is 2-3 orders of magnitude higher than common open ocean surface concentrations [*Dai and Martin*, 1995; *Gebhardt et al.*, 2005; *Hölemann et al.*, 2005; *Moore and Braucher*, 2008], even a small portion of the DFe in this water escaping the relatively high Arctic scavenging removal regime [*Cai et al., 2010*] could strongly affect surface DFe concentrations in the Central Arctic Ocean.

In this paper we present the distribution of DFe on the Arctic shelves (Barents, Kara and Laptev seas) and in the surface waters (upper 250 m) of the Central Arctic, obtained during the ARK XXII/2 expedition of *RV Polarstern* in August-September 2007 (Fig. 1). The multi-component approach using $\delta^{18}O$, salinity and nutrients as well as total alkalinity (A_T) measurements taken during the same cruise (see also *Bauch et al*. [2011 (in press)]) is used to study the influence of the different freshwater sources on the DFe distribution in the upper Arctic Ocean waters. The distribution of DFe in the deep waters of the Central Arctic Ocean is presented in a complementary manuscript by *Klunder et al*. [sub. man.].

2. Material and methods

2.1 Sampling and analysis

Water samples were collected during the ARK XXII / 2 expedition of *RV Polarstern* between 1 August and 23 September, 2007 (Fig. 1). At discrete depths, samples were taken using 24 internally teflon coated PVC 12 liter GO-FLO samplers (General Oceanics Inc.) mounted on a Titanium frame, which was connected to a Kevlar hydrowire [*De Baar et al., 2008*]. Inside a class 100 clean room environment samples for DFe analysis were collected from the GO-FLO bottles [*De Baar et al,* 2008]. Seawater was filtered using a 0.2 μm filter cartridge (Sartrobran-300, Sartorius) under nitrogen pressure. For each depth replicate samples of DFe were taken in 60 ml High Density Polyethylene (HDPE) sample bottles and acidified to pH = 1.8 with 12 M HCl (Baseline, Seastar Chemicals). Previously, all bottles, used for storage of reagents and samples, were acid cleaned according to a three step cleaning procedure, as described by *Middag et al.* [2009].

The DFe was measured using flow injection analysis with luminol chemiluminescence, where samples were buffered in-line to pH = 4, using a 0.12 M ammonium acetate buffer (pH =6.5). The DFe was pre-concentrated on an IDA Toyopearl AF-Chelate resin [*Klunder et al.,* 2010]. After pre-concentration, the column was rinsed (60 sec.) with ultrapure type 1 water and subsequently Fe was eluted from the column (120 sec.) using 0.4 M HCl (Merck Suprapur). Pre-concentration time was usually 120 seconds, except for the Laptev Sea stations, where a short loading time (15 sec) enabled determination of the very high concentrations present at this location.

2.2 Calibration and validation

97 The system was calibrated using standard additions of Fe to low DFe seawater. If an outlying
98 value for DFe was observed, the profiles of the other trace metals (dissolved aluminium (DAl)
99 and manganese (DMn)) and other nutrients (silicic acid, nitrate and nitrite, phosphate) were
100 evaluated for consistency with the regarded data point. In the case that no deviations were
101 observed in the other parameters and both the initial and duplicate sample showed an
102 exceptional value, the exceptional data point was considered as erroneous if the value
103 deviated more than +25 % from the expected profile based linear interpolation between the
104 DFe-concentration above and below the data point (after *Middag et al.* [*2009*] and *Klunder et*
105 *al*. [2010]). The total number of data points for DFe during ARK XXII/2 was 785. In total 5
106 data points were rejected, of which only 2 data points were situated in Arctic surface waters.
107 A table including stations, positions, date, depth, nutrient data, DFe data and total alkalinity is
108 available as an electronic supplement. The blank is the background concentration of DFe in
109 ultrapure type 1 water and chemicals and is defined as the concentration measured at 0
110 seconds loading time; the blank was 0.02 ± 0.02 nM (n= 41) on average and did not exceed
111 0.075 nM. The detection limit (3σ of the blank) was 0.07 nM or 70 pM. The amount of Fe
112 added to sample by addition of 12 M HCl (Baseline, Seastar) is < 0.4 pM per sample and is
113 considered negligible [*Klunder et al.* 2010].
114 The accuracy of the Fe flow injection analysis system was verified by regularly analyzing
115 SAFe D2 standard seawater. The results agreed well with the community consensus values:
116 0.92 ± 0.057 nM, n=24. (Certified consensus values are: 0.92 ± 0.03; www.geotraces.org).
117
118 *2.3 Other variables*
119 Samples for dissolved Mn (DMn) and dissolved Al (DAl) were simultaneously sampled with
120 those for DFe [*Middag et al.*, in press; *Middag et al.*, 2009]. At some stations, besides the Fe
121 in the dissolved fraction presented here, Fe was also measured in a smaller size fraction

(<1000kDa) and a "total dissolvable" fraction (unfiltered) [*Thuroczy et al.,* 2011 (in press)]. Salinity and potential temperature data were taken from the CTD profile.

Total Alkalinity (A_T) was determined by potentiometric titration in an open cell, according to the procedures outlined by *Dickson et al.* [2007]. Samples were collected in 250 ml borosilicate bottles and poisoned with 100 µl of a 50% saturated solution of $HgCl_2$ (i.e., to a concentration of 0.02%) and stored dark and cool, but without freezing, until analysis. All samples were analyzed during the expedition, most within 24 hours after sampling, with only a few stations within 72 hours of sampling. A correction factor of 1.0002 was applied to the results to compensate for the diluting effect of adding the $HgCl_2$ solution. Precision of the analysis, defined as the standard deviation of differences between duplicate analyses of certified reference material (CRM, batch 76, distributed by the Scripps Institution of Oceanography; [*Dickson 2001*]) is 1.5 µmol kg^{-1} (n=68). Analyses of CRM showed an initial bias of the instrument of about +0.3% (i.e., about 6 µmol kg^{-1}), which over the course of the cruise decreased to about +0.1% (i.e., about 2 µmol kg^{-1}). This minor inaccuracy and the gradual drift therein are corrected for in the results. The final dataset of A_T is accurate to ± 4 µmol kg^{-1}, this being approximately twice the standard deviation of the CRM measurements after the correction for bias and drift is performed.

Oxygen isotopes were analyzed at the Leibniz Laboratory (Kiel, Germany) applying the CO_2-water isotope equilibration technique on a Finnigan gas bench II unit coupled to a Finnigan DeltaPlusXL. At least 2 sub-samples were analyzed to reach an overall measurement precision for all $\delta^{18}O$ analysis of at least ±0.03‰ or smaller. For further details see *Bauch et al.* [2011 (in press)]. The $^{18}O/^{16}O$ ratio is given versus VSMOW in the usual δ-notation [*Craig*, 1961].

2.4 Calculation of river water and sea-ice meltwater fractions

147 Stable oxygen isotopes of the water in conjunction with salinity have proven to be a useful
148 and reliable tracer to identify and distinguish freshwater sources [*Östlund and Hut*, 1984].
149 Moreover, Atlantic and Pacific-derived waters within the marine fraction can be distinguished
150 and quantified based on nutrient concentrations (*Ekwurzel et al.*, 2001; *Jones et al.*, 1998,
151 2008; *Yamamoto-Kawai et al.*, 2008). The water mass fractions are calculated using either a
152 three component or a four-component system of mass balance equations based on salinity,
153 $\delta^{18}O$, and PO_4^*. The latter PO_4^* represents the initial phosphate concentration that accounts
154 for organic respiration of dissolved oxygen and is defined as
155 $PO_4^* = PO_4^{3-} + O_2/175 - 1.95 \cdot \mu molkg^{-1}$ [*Broecker et al.*, 1985]. In deep waters and below a
156 closed sea-ice cover at reduced O_2 air/sea exchanges, the PO_4^* is a quasi-conservative tracer
157 [*Ekwurzel et al.*, 2001]. The overall mass balance is governed by the following equations
158 [*Ekwurzel et al.*, 2001]:

159 $$f_a + f_p + f_i + f_r = 1 \quad (1)$$

160 $$f_a S_a + f_p S_p + f_i S_i + f_r S_r = S_{meas} \quad (2)$$

161 $$f_a \delta^{18}O_a + f_p \delta^{18}O_p + f_i \delta^{18}O_i + f_r \delta^{18}O_r = \delta^{18}O_{meas} \quad (3)$$

162 $$f_a PO^*_{4a} + f_p PO^*_{4p} + f_i PO^*_{4i} + f_r PO^*_{4r} = PO^*_{4meas} \quad (4)$$

163 where f_a is the fraction of Atlantic water, f_p the fraction of Pacific-derived water, f_i the fraction
164 of sea-ice meltwater (or brine influence if f_i is negative), and f_r is the fraction of meteoric
165 water for which the $\delta^{18}O$ signal is a suitable indicator. Meteoric water is all water ultimately
166 due to precipitation. In the Arctic Ocean, this can be supplied as river water or as local net
167 precipitation. River water and local precipitation are isotopically identical but river water
168 exceeds net precipitation [*Serreze et al.,* 2006], therefore we refer to this fraction as river
169 water. The S, O and PO_4^* with the corresponding subscripts are the endmember values and
170 measured values of salinity, $\delta^{18}O$ and PO_4^* [see *Bauch et al.,*2011 (in press)]. In the Atlantic

171 regime calculated fractions of Pacific-derived waters may be strongly negative, because of
172 endmember uncertainties and also due to a non-conservative behavior of dissolved oxygen
173 near the surface. In these cases, Pacific-derived water can be assumed to be absent and a 3-
174 component system of equations is solved (equations 1-3 with f_p set to zero). An alternative
175 calculation (similar to equations 1-4) using nitrate to phosphate ratios (N/P) facilitates the
176 differences in nitrate levels between Atlantic and Pacific-derived waters [*Jones et al.,* 1998,
177 2008; *Yamamoto-Kawai et al.,* 2008]. Comparison of Pacific-derived fractions from PO_4* and
178 N/P-based calculations are especially important for the interpretation of station data on the
179 Canadian Side of the Transpolar Drift (st. 338, 342, 345; Fig. 5). While the PO_4^* approach
180 generally tends to underestimate Pacific-derived waters due to non-conservative behavior O_2
181 near the surface, the N/P approach in the Transpolar Drift contains a seemingly Pacific signal
182 that in fact is originating from denitrification processes along the Siberian shelves [*Bauch et*
183 *al.,* 2011 (in press)].

184 A negative sea-ice meltwater fraction reflects the amount of water removed by sea-ice
185 formation and the absolute value is proportional to the subsequent addition of brines to the
186 remaining water column. All fractions are net values reconstructed from the $\delta^{18}O$ and salinity
187 signature of each sample and are the result of time integrated effects on the sample volume
188 over the residence time of the water. Uncertainties based on analytical errors are considerably
189 smaller than systematic and conceptual errors arising from limited knowledge of endmember
190 values. Systematic errors based on uncertainties in endmember salinity and $\delta^{18}O$ data remain
191 mostly within ±1% for river water and sea-ice meltwater fractions and uncertainties for
192 Pacific water fraction are up to about 10% for the PO_4*-based calculation [*Ekwurzel et al.*
193 2001] and up to 10% for the N/P-based method [*Yamamoto-Kawai et al.*, 2008]. For a
194 detailed discussion see *Bauch et al.* [2011 (in press)]
195

196 **3. Hydrographic background**

197

198 The largest inflow into the Arctic Ocean is Atlantic water, marked by high potential
199 temperatures (θ) (~3-5°C) and high salinity (~35) [*Rudels et al., 2001*]. This Atlantic water
200 enters the Arctic Ocean in two branches. One branch flows through the Fram Strait and then
201 eastwards along the Siberian continental margin at a depth of ~200-600 m [*Rudels, 2001*].
202 The other branch flows over the Barents Sea and Kara Sea and joins the Fram Strait Branch at
203 St Anna Trough [*Rudels,* 2001]. The dominant surface current across the Central Arctic
204 Ocean is the Transpolar Drift (TPD), fed by surface waters from the Laptev and East Siberian
205 seas. The TPD crosses the Central Arctic Ocean, and leaves the basin southward through
206 Fram Strait and there constitutes forms the East Greenland Current [*Rudels,* 2001; Fig 1a].
207 Throughout the Arctic, the upper surface waters are strongly influenced by a major
208 freshwater input from the Siberian and North American rivers, by Pacific inflow through
209 Bering Strait and by melting of sea-ice [*Aagaard and Carmack,* 1989]. This results in a
210 surface mixed layer (SML) marked by minima of salinity and potential temperature. During
211 ARK XXII/2, the mixed layer (defined as the shallowest depth deeper than 10m where σ-σ_{10m}
212 < 0.05 (after *Rintoul et al.* [2001])) varies between 11-25 m over the study area. During the
213 Ultraclean CTD casts, in many cases the shallowest sample measured was situated below the
214 SML. Below the SML, upper halocline waters (UHW) are marked by a nutrient maximum
215 and are most pronounced in the Makarov basin at salinities of about 32.5-33.5 (e.g. [*Guay and*
216 *Kenison Falkner*, 1997]). The lower halocline waters (LHW), observed in all Arctic basins,
217 are originally formed by winter convection in the Nansen Basin [*Rudels et al.*, 2004] and
218 intrusions of saline shelf water [*Steele and Boyd, 1998*], causing higher salinities 34-34.5
219 (e.g. [*Guay and Kenison Falkner*, 1997]) compared to the UHW. *Steele and Boyd* [1998]
220 mention the formation of halocline waters in the Makarov Basin as a result of large amounts

of freshwater leaving the Laptev Shelf Continental Margin. Below the halocline, Atlantic derived waters are observed, marked by a temperature maximum and higher salinity of about 34.92 in the south western Nansen Basin [*Aagaard et al.*,1981]. In this study, the Surface Layer Waters (SLW) comprise the SML, UHW and LHW and are defined as waters with salinity < 34.5 (after [*Guay and Kenison Falkner*, 1997]).

4. Results

For all stations occupied during ARK XXII/2, the average DFe concentrations in the SLW together with isohalines are shown in Fig. 1a. Positions of transects are depicted in Fig. 1b. Since there is a clear correlation between DFe and salinity in the upper Arctic Ocean, the fractions of the different freshwater sources are displayed together with DFe (Figures 3-6) as they may give information about the different sources of Fe in the Arctic Ocean.

4.1 Shelf Seas

For the shelf seas, depth profiles of DFe, together with light transmission and salinity, are depicted in Fig. 2. In the Barents Sea (Fig. 2a; Fig. 3) high Fe (>1 nM) and salinity (>35.1) was found in the upper layer (25-50 m) southernmost station (228). Below a DFe enrichment in surface waters, stations 236 and 239 showed a subsurface minimum at ~50m water depth (also at station 237), which corresponded to a maximum of fluorescence. Below 50m, the DFe concentrations were relatively constant with depth (0.6-0.8 nM). The fractions of river water were relatively low in the Barents Sea and some sea-ice meltwater was observed in the upper water around station 239 (Fig. 3).

Four stations were occupied north-east of Franz Josef Land, over the St Anna Trough and at the Kara Sea slope (Fig. 1b and profiles in 2b). All stations showed a surface depletion of DFe in the upper 10 m and a pronounced subsurface maximum at 25 m depth. At all

246 stations this layer was marked by reduced temperature θ (not shown), relatively low salinity
247 (<33.5), higher fluorescence (Fig. 2b) and some river water (up to 3%) as well as sea-ice
248 meltwater (2-5%) was observed (Fig. 4). Below the DFe minimum at 25 m depth there was an
249 enrichment at 75 m and below that a relatively low (0.4-0.5 nM) DFe concentrations (st
250 271/272) or a depletion at 75 m (st 276) and below that a relatively higher DFe (0.5-0.6 nM)
251 (st 276/279).

252 Two stations (407 and 411) were occupied in the shallow Laptev Sea (Fig 2c). In the
253 upper 10 m the DFe concentrations of ~3 nM coincided with low salinity and correspondingly
254 high fractions of river water (12–14%) and some sea-ice meltwater (~3%). Below the low
255 salinity layer low DFe concentrations (<2 nM), sea-ice meltwater and river water
256 contributions were found at station 407. At station 411, closer to the shelf edge, high DFe
257 concentrations (>10 nM) corresponded to higher salinity and lower light transmission (Fig.
258 2c), and a strong influence of brine waters (negative sea-ice meltwater fraction; fi~-9%).
259 Relatively high river water fractions (~15%) were observed.

260

261 *4.2 Surface waters in the Central Arctic Basin*

262 There was a strong relation between high DFe and low salinity in the Eurasian Basin and
263 Central Arctic (Fig. 1a), where in the south western Nansen Basin low concentrations of DFe
264 corresponded to high salinity and in the Amundsen and Makarov Basins increasing DFe
265 corresponded to decreasing salinity. An exception to this inverse correlation pattern between
266 salinity and DFe was the region above the Alpha Ridge: here at stations 338 and 342 (Fig. 1a),
267 which we assume to be just outside the influence of the Transpolar Drift, salinity further
268 decreased but also DFe concentrations were low. The position of the Transpolar Drift is
269 inferred from the distribution of Pacific-derived waters and extrema of river water and
270 negative sea-ice meltwater fractions (see discussion in *Bauch et al.* [2011 (in press)]).

271 Moreover,the enhanced transport rates inferred from transient tracer evidence support this
272 position of the TPD [*van der Loeff et al.*, man. sub.].

273 In the western part of the Nansen Basin (Transects 1 and 2), the concentrations of DFe
274 were generally low in the upper surface, despite some freshwater from sea-ice meltwater and
275 river water (Fig. 3, 4). In the northernmost station of transect 1, the DFe increased with
276 increasing river water (Fig. 3), whereas further east, at the northernmost station of transect 2,
277 high river water and low DFe was found (Fig. 4). The western part of the Nansen Basin had
278 relatively low fractions of river water and sea-ice meltwater (with a total always <6%) in the
279 upper surface. Sea-ice meltwater was mostly restricted to the upper 25 m where DFe was
280 generally low (<0.5nM). Although river water was present (2-3%) over most of the western
281 Nansen Basin, the river influence was very low (<1%) at the shelf break just north of Franz
282 Josef Land (Fig. 4).

283 Further east at the Kara Sea slope, increasing river water fractions and about constant
284 sea-ice meltwater fractions coincided with relatively higher DFe (Fig. 4; ~0-150 km of
285 section). In the central Nansen Basin both the DFe concentrations (~0.5 nM) and the river
286 water fractions were relatively low (Fig. 5; see section at ~150-400 km).

287 Relatively high surface DFe concentrations were observed above the Gakkel Ridge
288 together with large fractions of river water and some influence of brine waters (i.e. negative
289 sea ice-meltwater fractions) (Fig. 6). In the Nansen Basin near the Laptev Sea margin, the
290 surface DFe concentrations decreased as well as the fractions of river water and sea-ice
291 meltwater (Fig. 6; ~600-800 km of section). Towards and onto the Laptev Sea shelf (see
292 section 4.1 and Fig. 7) both the DFe concentrations and river water fractions increased again.

293 Towards the Amundsen Basin an increase was observed in the DFe concentrations that
294 coincides with high river water fractions (>10%) and sea-ice formation (negative sea-ice
295 meltwater fraction) (Fig. 5; see section at ~600-100 km and at ~2500 km). This pattern was

observed somewhat more pronounced, in the Makarov Basin further west (Fig. 5, see section at ~1100-1500 km and 2000-2400 km). A considerable influence of Pacific water (>20%) was observed in the entire Makarov Basin. On the North American side of the Transpolar Drift, Pacific-derived waters comprised a major fraction of the upper water column seen most pronounced at station 342 with f_p~90% (Fig. 5). The maximum in Pacific fractions coincides with a strong DFe minimum, observed for all stations on the North American side of the TPD.

5. Discussion

The inverse linear relationship between DFe and salinity (Fig. 8a) demonstrates the important role of Arctic rivers in the delivery of DFe to the Arctic Ocean. Nevertheless, significant deviations from the linear trend indicate that there are also other important sources and processes. In the following discussion we first compare our results with existing (D)Fe data from the Arctic (5.1) and discuss the processes on the shelf seas (5.2). Then we discuss the concentration of DFe in freshwater sources (5.3) and compare the distribution of DFe in the central Arctic Ocean with the distribution of freshwater (5.4). Processes involved in sea-ice formation and transport will alter the ratio of total Fe (TFe) and the dissolved fraction (DFe). Therefore, in order to understand the impact of these sea-ice processes on the Fe distribution the ratio TFe/DFe is discussed (5.5).

5.1 Comparison with previously published data

Our study shows that concentrations of DFe in Siberian shelf seas are relatively low (<1 nM), except for the Laptev Sea where rather high concentrations (> 10 nM) are observed. In the Central Arctic, concentrations vary from ~0.5 nM in the Nansen Basin, to >2nM in the Amundsen and Makarov basins. To our knowledge no other data has been previously reported

for dissolved (0.2 μm filtered) DFe in the Arctic Ocean, but there are some studies reporting unfiltered Fe concentrations. Our observations are consistent with data of *Moore et al.* [1983], who reported a profile with ~1.5 nM of reactive iron in the surface waters above the Lomonosov Ridge. *Measures* [1999] reported generally higher concentrations in the range of 0.67-20 nM for reactive Fe on a transect across the Arctic Ocean, with 1.55-3.5 nM over the Lomonosov Ridge and the Makarov Basin and 0.67-1.31 nM for the western Nansen Basin. These ranges of unfiltered samples are slightly higher than the data presented here for filtered samples, but agree well with the values for unfiltered samples from our same casts [*Thuroczy et al.,* manuscript submitted]. *Tovar-Sanchez et al.* [2009] reported Fe concentrations of 10 ±1.8 nM (n=10) in upper surface waters (1 m depth) just north of Spitsbergen and values are thereby roughly an order of magnitude higher than our data sampled slightly to the east at ~15-20° (see Fig. 2, 3). However, the difference may be at least partly explained by the fact that *Tovar-Sanchez et al.* [2009] reported unfiltered Fe and sampled at ~1 m water depth to specifically capture the influence of melting of sea-ice. In contrast filtered (dissolved) Fe concentrations reported here are from > 10 m water depth.

5.2 Shelf seas

In the Barents Sea, all stations show a subsurface DFe minimum, often coinciding with a maximum in fluorescence (Fig. 2a). This fluorescence is due to presence of chl a, and may indicate uptake of DFe by phytoplankton. *Cai et al.* [2010] report a relatively high POC export in the Barents Sea from measurements collected on the same expedition, indicating significant primary production in the months before the expedition. Indeed, NASA SEAWifs images show high concentrations of chlorophyll (~5 mg m^{-3}) in the Barents Sea in the months before our cruise (May-June) [*Feldman and McClain*, 2011]. During our expedition concentrations had already decreased to (< 1 mg m^{-3}) (NASA SEAWifs images [*Feldman and*

346 *McClain*, 2011]) (Fig. A1). Moreover, the chl a distribution in the Barents Sea shows
347 variations of one order of magnitude in the region southeast of Spitsbergen in June-July 2007.
348 Also satellite derived annual primary production data of the calendar year 2007 from the
349 Arctic Ocean, show variations between 50-150 g C m^{-2} yr^{-1} over the Barents Sea Shelf [*Arrigo*
350 *et al.*, 2008]. Therefore, it is likely that biological uptake and depletion of DFe in the months
351 prior to the expedition has led to the observed low concentrations. Of the four Barents Sea
352 stations, station 237 has the lowest POC export [*Cai et al.*, 2010] and relatively higher DFe,
353 suggesting little DFe depletion by phytoplankton at this station, consistent with spatial
354 variation within the Barents Sea (Fig. 3). The very high DFe concentration (~1.67 nM) close
355 to bottom depth at station 236 is consistent with a similar high concentration observed in
356 DMn distribution and is attributed to benthic efflux [*Middag et al.*, 2011]. The Kara Sea
357 stations differ from the Barents Sea and Laptev Sea shelf sea stations as they are situated all
358 on the outer shelf, close to the slope, rather than on the central shelf (Fig. 1b, inset). All Kara
359 Sea stations show an upper surface biological depletion in DFe, consistent with the maximum
360 chl a fluorescence signal in the upper 20 m surface water (Fig. 2b). Station 271, situated
361 furthest from the shelf, shows a small intrusion of cold, fresher, slightly less oxygenated
362 waters (Fig. 2b), likely from the shelf, below a stable mixed layer (upper 15 m). Higher DFe
363 in these advected shelf waters may explain the higher DFe in the upper 25 m at station 271.
364 Similarly, an even stronger decrease in salinity and oxygen may indicate intruding waters
365 from the shelf at station 279, and thus explain the high DFe concentrations, although this is
366 not confirmed in the θ profile (Fig. 2b). Below the upper 50 m the Atlantic core is recognized
367 by higher θ and salinity; at station 271 and station 279 at ~ 75 to 175 m water depth. At
368 stations, 272 and 276, situated further from the shelf, a deeper Atlantic water layer is
369 observed. Below 100 m, the slightly lower DFe at station 271 and 272 (~0.4-0.45 nM) may be
370 due to influence of Fram Strait Branch Waters, whereas the DFe at station 276 and 279 (~0.5-

371 0.55 nM) may be influenced by Barents Sea Branch Waters (Fig. 4). In general, the DFe
372 concentrations are slightly lower in the Kara Sea than in the Barents Sea; DFe may be
373 removed during transport from the Atlantic source to the Kara Sea both by adsorptive
374 scavenging removal and/or biological uptake. Remarkably, the profile of dissolved Barium
375 (Ba) as measured at station 276 follows a reverse pattern as DFe at this depth, with a small
376 decrease at ~100-125 m. [*Roeske et al.,* subm. man.*,* their Fig. 4]. It may be possible that some
377 small influence of advected shelf waters with a (small) sea-ice meltwater signal at ~100-125
378 m depth causes the lower Ba [*Roeske et al.,* subm. man.] yet higher DFe concentrations.
379 Although these data do not provide a definitive conclusion, our suggestion of advected water
380 with elevated sea-ice meltwater influence is consistent with the deviations observed in the
381 salinity profile (Fig. 2b), high dissolved Al at a depth of 125 m [*Middag et al., 2009*] and the
382 higher $\delta^{18}O$ (not shown) at these depths. The DFe concentrations gradually decrease at
383 Station 276 below 300 m to ~0.45 nM at 620 m depth

384 In the Laptev Sea (station 411; see Fig. 7) a very low light transmission signal is found
385 below 20 m, corresponding to extremely high DFe. Because low light transmission indicates
386 presence of particles, local resuspension from bottom sediment may be an input source for
387 DFe (Fig 2c). Moreover, these enhanced DFe concentrations in the bottom waters may come
388 from the rapid regeneration at depth of organic material exported from the upper waters. This
389 mechanism has been reported for dissolved Barium (Ba) that shows a similar distribution with
390 high concentrations in Laptev Sea bottom waters [*Abrahamsen et al.*, 2009; *Roeske et al*.,
391 subm. man.]. Organic matter in this part of the Laptev Sea is mainly of terrestrial origin
392 [*Anderson et al.*, 2009]; the dissolution of this organic matter may explain the observed high
393 concentrations of DFe. Additionally, bottom waters on the Laptev Sea shelf are known to
394 contain some river water and are also influenced by sea-ice formation (Fig. 7) [*Bauch et al.*,
395 2009]. Since river water fractions do not differ as much between surface and bottom layer

(Fig. 7) the extremely enhanced DFe concentrations in the bottom layer are not primarily determined by river contribution. Brine rejection from sea-ice formation may be of importance in distributing DFe over the water column. For the Weddell Sea, *Lannuzel et al.*[2008] reported DFe enrichment upon brine drainage. Close to the shelf edge, the station 407 shows relatively lower DFe and higher salinity, than station 411 on the shelf (Fig. 2c), due to the Atlantic Boundary Current flowing along the Arctic shelf seas [*Rudels et al.*, 2004] transporting saline water with relatively low DFe [*Klunder et al.*, manuscript submitted] onto the outer Laptev Sea shelf.

5.3 Fe in freshwater sources

The inflow of river water is a major source of DFe to surface waters. The DFe concentrations in Arctic rivers vary considerably. *Dai and Martin* [1995] reported 250 -650 nM for the Ob and Yenisey rivers and *Hölemann et al.* [2005] reported a range of 410-7132 nM for the Lena river. Concentrations of DFe in river water are seasonally variable: both the North American and Eurasian rivers show a strong seasonal summer peak in their discharge volume with higher DFe concentration during the peak discharge [*Rember and Trefry*, 2004; *Hölemann et al.*, 2005]. These concentrations are orders of magnitude higher than common ocean seawater concentrations, however a large amount of DFe is expected to be removed by precipitation/flocculation and sinking in the estuaries [*Boyle et al,.* ,1977].

The melting of seasonal sea-ice is another possible input source of DFe [*Measures*, 1999]. In the Southern Ocean, melting of seasonal sea-ice has been shown to cause enrichment of DFe [*Klunder et al.,* 2010; *Lannuzel et al.*, 2008]. It is important to note that the DFe concentration in sea-ice can be modified by biological processes (uptake by phytoplankton and bacterial remineralisation) [*van der Merwe et al.*, 2009]. Also Arctic sea-ice may receive Fe from atmospheric sources [*Darby et al.*, 1974]. However, because the

Arctic sea-ice is largely formed on the Arctic shelves, the entrainment of sediments, either from rivers or suspension at the shelf can be assumed to be a more significant process [*Nürnberg et al.*, 1994]. *Hölemann et al.* [2005] reported very high (281-10585 nM) DFe concentrations in sea-ice in the Laptev Sea, where the concentrations near the Lena River Delta exceeded the concentrations further on the shelf by two orders of magnitude. *Tovar-Sanchez et al.* [2009] reported concentrations of 532-864 nM total dissolvable Fe in Arctic sea-ice for stations north of Spitsbergen. This wide range of Fe enrichment in samples taken relatively close to each other illustrates the strong spatial variability of the input of sea-ice derived particulate and dissolved Fe, that will lead to patchiness in the distribution of DFe in Arctic sea-ice meltwater and consequently in the water below.

Moreover, the contribution of dissolved Fe to the total Fe in sea-ice cores has been shown to vary between less than 1% to 33% in the Subarctic Bering Sea [*Aguilar-Islas et al.*, 2008]. This stresses the role of release mechanisms and dissolution processes in delivery of dissolved Fe from sea ice sediments to the water column [*Cámara-Mor et al.*, 2010; *Nürnberg et al.*, 1994]. The Transpolar Drift (TPD) carries sediment laden sea-ice to the Central Arctic where it can be released upon melting [*Cámara-Mor et al.*, 2010; *Nürnberg et al.*, 1994]. It is important to note that the mass balance equations used in this study yield a net value of the sea-ice contribution over the residence time of the water and melting as well as formation may have taken place before the time of measurement. Therefore water with a negative value for the fraction sea-ice meltwater (reflecting net sea-ice formation) may still contain some recent addition of sea-ice meltwater, i.e. may still have a sea-ice related DFe source.

In the Makarov Basin, a large part of the freshwater component is due to waters of Pacific origin. This water may contain a different DFe signature compared to the marine waters in the Eurasian Basin that consist primarily of Atlantic-derived waters [*Bauch et al.,* 2011 (in press)]. The DFe concentrations in the surface waters of the North Pacific vary widely (0.1

446 nM - 3 nM) [*Takata et al.*, 2004; *Moore and Braucher*, 2008; *Aguilar-Islas et al.*, 2008].
447 Besides this wide range in concentration of DFe in the North Pacific Ocean, there is
448 significant biogeochemical modification of Pacific Waters during transit over the shallow
449 shelves from the Bering Sea to the central Arctic [*Codispoti et al.*, 2005] (transit time in the
450 order of 1-6 months [*Woodgate et al.*, 2005]). Therefore, the DFe endmember concentration
451 in Pacific-derived waters in the Arctic Ocean halocline has a wide range and cannot be
452 defined as one single end-member value.
453
454 *5.4 DFe concentration in correlation to freshwater distribution*
455 The strong linear relationship between DFe and river water in the surface layer of the Central
456 Arctic (Fig. 8b) indicates that river water is the most important DFe source in the Central
457 Arctic Ocean. The DFe concentration does not exceed 1.5 nM in regions with river water
458 fractions <10 %, whereas in regions with >15% river water fraction, DFe concentrations of up
459 to 3 nM are found..
460 The small portion of total freshwater (river water and sea-ice meltwater <~6%) present
461 in the Eastern Nansen Basin and over the Barents Sea and Kara Sea shelves does not show a
462 clear correlation with the distribution of DFe. Sea-ice meltwater contributes about half of this
463 freshwater but no related increase in DFe is observed (Figs. 3, 4). Thus sea-ice meltwater is
464 generally not a significant source of DFe in this region. At the northernmost station of transect
465 1 (Fig 3) and east of the St. Anna Trough (Fig. 4) small but significant input of river water
466 correlated with high DFe. This river water originates from shelf regions further east where it
467 becomes frozen and next transported as ice together with sea-ice [Bauch et al., 2011 (in
468 press)], and it melts again in the Barents Sea and eastern Nansen Basin. The DFe present in
469 this river water transported as ice may be subject to biological Fe-depletion during transport
470 causing strong spatial variation in concentrations of DFe (see section 5.3). Also, both the

471 strong surface depletion in phosphate (Fig. A2) and the relatively high POC-export fluxes
472 (1.7-5.5 mmol m^{-2} d^{-1}) [*Cai et al.*, 2010] indicate phytoplankton growth and subsequent export
473 in the months prior to our expedition (see section 5.2). If this production would take up the
474 DFe from sea-ice meltwater it would not be observed in the DFe concentrations despite
475 considerable river water and sea-ice meltwater fractions. The facts that melting of sea-ice in
476 the Barents Sea commenced in mid-May 2007 [*Spreen and Kaleschke, 2008*] and our
477 sampling in the Barents Sea took place at the end of July 2007 are in favor of such a
478 mechanism, which was also observed in the Ross Sea [*Sedwick and DiTullio*, 1997].
479 The two stations at the North American side of the TPD (station 338 and 342, Fig. 1a)
480 significantly deviate from the correlation between DFe and river water fractions seen in the
481 Eurasian Basin and in the TPD (Fig. 9). While river water fractions are lower compared to
482 values found in the TPD, still significant river water fractions are observed which are not
483 reflected in the actually low DFe concentrations (Fig. 5). At stations 338 and 342 an
484 enrichment of DFe is observed at the surface, lower DFe concentration at the subsurface and
485 another DFe-enrichment at 75-100 m depth (Fig 9). Salinity at these stations is low at the
486 surface, but increases in the upper 30 m, remains relatively constant between ~30-60 m depth
487 and continues to increase below (Fig. 9). Compared to salinity values found at ~60 m an
488 additional input of 1-2% freshwater (S=0) is needed to obtain the low salinity values found in
489 the upper 30 m. Moreover, there is a DFe decrease of 0.32 nM from 10 to 50 m and of
490 0.15 nM from 10 to 25 m for station 338 and 342 respectively. Although the fraction of
491 (Eurasian) river water is high compared to that of sea-ice meltwater (8-10%), the river water
492 fractions are relatively constant over the upper 50 m, whereas positive sea-ice-meltwater
493 fractions (~3%) are only observed in the shallowest sample (~10 m) and are consistent with
494 the high DFe concentrations. From the lower salinity in the upper ~10 m, relative to the
495 winter mixed layer salinity and the observed relation of high DFe with sea-ice meltwater it is

496 suggested that the low salinity, high DFe input comes from the surface. Assuming DFe
497 enrichment is caused solely by sea ice meltwater, the DFe endmember concentration is
498 calculated using the extra sea-ice meltwater input of 2% and 1.5 % and the DFe decrease of
499 0.32 and 0.15 nM respectively. The DFe-concentration for the sea-ice meltwater endmember
500 should thereby be ~16 nM and ~10 nM DFe, for stations 338 and 342 respectively. This
501 calculated DFe concentration for the sea-ice endmember is low compared to the reported DFe
502 in Arctic sea-ice (see section 5.3). However, we may expect strong spatial variations in the
503 amount of DFe released from melting of sediment laden sea-ice as it is dependent on the
504 amount of sediment contained in the ice and on the dissolution mechanisms. The presence of
505 chlorophyll a in the upper 50 m [*Cai et al., 2010*], may point to biological depletion causing
506 the lower DFe concentrations at ~25-50m depth. Instead of North American river water,
507 *Roeske et al.*, [subm man.] attributed the waters at 50-100 m depth to halocline waters from
508 the Chukchi Shelf, carrying the properties of mineralization processes between bottom waters
509 and sediment. This is reflected in high Ba concentrations [*Roeske et al.*, subm man.] and low
510 O_2 and high silicate concentrations (Fig. 9). These mineralization processes could cause the
511 DFe increase from 50m to ~100 m at station 338 and 342. The strongest influence of these
512 waters from the Chukchi Sea is found at 100 m depth at station 342 as reflected in the Si
513 maximum (Fig. 9) and may explain the high DFe concentrations here. In contrast, lower DFe
514 concentrations (Fig. 9) at station 338 may be caused by mixing with Atlantic waters, which
515 comprise already >60% of the water mass at 100 m. Below ~125 m, the DFe decreases (Fig.
516 9), consistent with the DFe concentration observed in the deep waters of the Makarov Basin
517 [*Klunder et al.,*manuscript submitted].
518 An alternative explanation for the relatively low DFe values on the North American
519 side of the TPD is the longer transit time of waters from the shelf seas to the Central Arctic in
520 the Beaufort Gyre compared to the fast transport of river derived waters from the shelf to the

521 Central Arctic by the TPD. This longer transit time would allow more Fe to be removed by
522 scavenging processes. In addition, DFe may be taken up by phytoplankton in the preceding
523 months, enhanced by the largely ice-free conditions in 2007 in this part of the Canadian Basin
524 [*Arrigo et al.*, 2008].

525 A small subset of stations were also sampled for total alkalinity (A_T) . The A_T data
526 supports the finding that the low salinity (and high DFe input) within the TPD is caused by
527 (mixing with) Eurasian river water, whereas the stations on the North American side of the
528 TPD have a different freshwater signature. In Fig. 10 the A_T vs salinity relationship is
529 depicted, including the mixing lines between Atlantic, Pacific, North American river water
530 and Eurasian river water endmembers (see caption for endmember values). The DFe
531 concentrations are shown in color. The high A_T, high salinity waters with low/moderate DFe,
532 are mainly Nansen Basin waters. As aforementioned, some stations in this region are
533 influenced by sea-ice meltwater (following grey arrow, Fig. 10). A decrease in A_T and salinity
534 is seen at ~50 m (shallowest sampling depth for A_T) in the stations within the TPD (green
535 ellipse), where also DFe concentrations increase. Remarkably, these datapoints lie between
536 the Atlantic Water/Eurasian river water and Atlantic Water/Northamerican river water mixing
537 lines. Substantial ice formation, as has been observed in the TPD (Fig.5), would result in the
538 observed devation from the Atlantic Water/Eurasian river water mixing line. Nevertheless,
539 influence of Northamerican rivers to the TPD cannot be ruled out. There are two data points at
540 ~50 m depth on the North American side of the TPD, showing a lower A_T relative to their
541 salinity than within the TPD (orange ellipse). These data points are on the mixing line of
542 Eurasian river water and Pacific Water (Fig. 10). This is consistent with the observed river
543 water fractions of ~6-8 (Fig. 5) and influence of Pacific water flowing over the Chukchi Shelf
544 (see section 5.3 and *Roeske et al.,* [subm man.]). *Anderson et al.* [2004] noted that biological

545 processes little affect the A_T in the Arctic Ocean which is in line with little change observed
546 in A_T concentrations during transit over the Chukchi shelf.
547 .
548 *5.5 Dissolved vs. total dissolvable Fe: implications for Fe delivery to the Arctic*
549 Recent melt of sediment laden sea-ice or influx of riverine sediments from the shelves would
550 result in a high concentration of Fe in the particulate phase and thus a relatively high
551 unfiltered (total dissolvable) Fe concentration (TDFe). During transit from the shelves to the
552 Central Arctic, dissolution processes, sinking and particle scavenging will lower the ratio of
553 TDFe relative to DFe. Thus the ratio TDFe/DFe may give insight in these processes. For
554 instance a rapid removal of TDFe compared to DFe with offshore distance from the Antarctic
555 Peninsula was observed [*Ardelan et al.*, 2010] indicating strong settling loss of TDFe relative
556 to DFe in surface waters. Fig. 11 shows the TDFe/DFe ratios versus salinity in the upper 100
557 m for stations on the Siberian shelves and for open ocean stations. Generally, the TDFe/DFe
558 ratios are lower for open ocean stations than for shelf stations (closed and open dots in Fig.
559 11, respectively). The higher ratio at shelf stations indicates a strong and recent input of
560 sediments, released during local melting of sea-ice or from rivers and causing very high Fe
561 concentrations in the size fraction >0.2 μm. We suggest that recent local sea-ice meltwater
562 was not present in the Central Arctic Ocean and that during transit from the shelf seas to the
563 central Arctic Ocean most of the Fe in the particulate fraction is removed, resulting in
564 TDFe/DFe ratios close to 1 at these stations (Fig.11). In sea-ice cores from the Bering Sea the
565 TDFe/TFe ratio is between 2.6-1800 (median 42) [*Aguilar-Islas et al.*, 2008], close to the
566 TDFe/DFe ratios observed for shelf stations rather than to those observed in the Central
567 Arctic (Fig.11). This strengthens our concept that river water rather than meltwater of
568 sediment laden sea-ice is the dominant DFe input source in the central Arctic Ocean. In
569 principle the melting of possibly sediment laden sea-ice at stations 338 and 342 should be

570 visible in high TDFe/DFe ratios. Unfortunately this remains speculative because no TDFe
571 measurements are available from stations 338 and 342.
572

573 **6. Summary and conclusion**

574 The data reveal that the DFe distribution throughout the surface waters of the central Arctic
575 Ocean is largely correlated with freshwater input sources, which is predominantly Eurasian
576 river water. On the shelves other factors influence the Fe distribution. In the Barents Sea and
577 Kara Sea, DFe minima at high chl a concentrations indicate DFe depletion by phytoplankton
578 growth. Strong carbon export and high chlorophyll abundance from satellite images indicate
579 that it is likely that DFe input enabled primary production in the months prior to our cruise.
580 This input likely comes from sea-ice meltwater and ice transported river water in the Barents
581 Sea. Biological depletion of DFe could then explain the relatively low DFe concentrations
582 despite significant sea-ice meltwater and river water signals. Very high DFe concentrations
583 near the bottom of the Laptev Sea are attributed to either sediment resuspension, sinking of
584 brine, or regeneration of Fe in the bottom layer.

585 In the central Arctic, both the Atlantic boundary current and the Transpolar Drift
586 transport DFe within Arctic surface waters. The DFe concentration in the western part of the
587 Eurasian Basin reflects mainly the concentrations of Atlantic surface water. The influence of
588 Atlantic water can still be recognized at the Laptev Sea continental margin, in high salinities
589 and relatively low DFe. Freshwater from the Eurasian rivers mainly transported by the TPD is
590 the main contributor to DFe in the Amundsen and Makarov basins, where DFe concentrations
591 > 2nM are observed. Here, the ratios of dissolved relative to “total dissolvable” Fe are low,
592 likely due to dissolution of DFe and scavenging/sinking of DFe in the “total dissolvable”
593 fraction. Above the Mendeleev-Alpha Ridge, on the North American side of the Transpolar
594 Drift, two stations deviate from the pattern of river transported DFe. Here the DFe

595 concentrations are generally lower than those within Surface Layer Water of the TPD. This
596 may be caused by the presence of Pacific-derived waters having lower DFe concentrations
597 due to biological depletion during transit, but also by (Eurasian) river water with longer
598 residence times compared to river water in the Eurasian Basin and the TPD. Scavenging and
599 uptake by phytoplankton during transport from the shelves may lower DFe concentrations.
600 Mixing of river water with Atlantic- and Pacific-derived waters within the TPD and on the
601 North American side of the TPD, respectively is also observed from the distribution of Total
602 Alkalinity. More specifically, the DFe concentrations on the North American side of the
603 Transpolar Drift are strongly determined by sea-ice meltwater in the upper 50 m. A significant
604 influence of remineralisation is seen DFe enrichment at ~ 100m depth , However, generally
605 biological depletion of these waters during transit over the shelves results in a overall low
606 DFe concentration.

607 The results suggest that shifts in delivery of DFe to the Arctic Ocean with regard to
608 the regional change in climate may primarily depend on shifts in Arctic currents (e.g. shift in
609 the position of the TPD) and on the amount of river runoff rather than on an expected further
610 increase in sea-ice meltwater. However, loss of Arctic sea-ice cover also alters an important
611 transport mechanism of river derived DFe within the Arctic Ocean and specially the Arctic
612 shelf seas, which are the most productive areas [*Pabi et al.*, 2008]. Recently *Arrigo et al.*
613 [2008] suggested an increase in denitrification in the Arctic Ocean, resulting in a further
614 depletion of the already low nitrogen concentrations in the waters leaving the Arctic to the
615 North Atlantic, this likely enhancing N_2 fixation in the North Atlantic [*Arrigo et al.*, 2008;
616 *Yamamoto-Kawai et al.*, 2006]. This raises the question whether the Fe concentrations in the
617 waters transported from the Arctic to the North Atlantic would contain enough Fe, which is
618 reported to be a control factor for N_2 fixation [*Falkowski et al.*, 1998], to sustain such
619 enhanced N_2-fixation. Based on the results of this study, we may carefully confirmthe

relatively high concentration of DFe in the waters exiting the Arctic relative to the lower DFe in common North Atlantic surface waters [*Moore and Braucher*, 2008].

7.Acknowledgements

This work was funded by BSIK under grant xxxx. DB was funded under grant SP526/3 by the German Research Foundation (DFG). Special thanks to Karel Bakker for nutrient analysis and Lorendz Boom for technical assistance. We are grateful to crews and colleagues onboard of RV Polarstern.

8. References

Aagaard, K., L. K. Coachman, and E. Carmack (1981), On the halocline of the Arctic Ocean, *Deep Sea Research Part A. Oceanographic Research Papers*, *28*(6), 529-545.

Aagaard, K.and Carmack, E.C. (1989), The role of Sea Ice and Other freshwater in the Arctic Circulation. Journal of Geophysical Research – Oceans, 94(C10):14485-14498.

Abrahamsen, E. P., et al. (2009), Tracer $\delta^{18}O$ derived freshwater composition of the Siberian continental shelf and slope following the extreme Arctic summer of 2007, *Geophys. Res. Lett.*, *36*(7), L07602.

Aguilar-Islas, A. M., R. D. Rember, C. W. Mordy, and J. Wu (2008), Sea ice-derived dissolved iron and its potential influence on the spring algal bloom in the Bering Sea, *Geophys. Res. Lett.*, *35*(24), L24601.

Anderson, L., G. Björk, O. Holby, E. Jones, G. Kattner, K. Koltermann, B. Liljeblad, R. Lindegren, B. Rudels, and J. Swift (1994), Water masses and circulation in the Eurasian Basin: Results from the Oden 91 expedition, J. Geophys. Res., 99, 3273–3283.Anderson, L. G., S. Jutterström, S. Kaltin, E. P. Jones, and G. Björk (2004),

644 Variability in river runoff distribution in the Eurasian Basin of the Arctic Ocean, *J.*
645 *Geophys. Res.*, *109*(C1), C01016.
646 Anderson, L. G., S. Jutterström, S. Hjalmarsson, I. Wåhlström, and I. P. Semiletov (2009),
647 Out-gassing of CO2 from Siberian Shelf seas by terrestrial organic matter
648 decomposition, *Geophys. Res. Lett.*, *36*(20), L20601.
649 Ardelan, M. V., O. Holm-Hansen, C. D. Hewes, C. S. Reiss, N. S. Silva, H. Dulaiova, E.
650 Steinnes, and E. Sakshaug (2010), Natural iron enrichment around the Antarctic
651 Peninsula in the Southern Ocean, *Biogeosciences*, *7*(1), 11-25.
652 Arrigo, K. R., G. van Dijken, and S. Pabi (2008), Impact of a shrinking Arctic ice cover on
653 marine primary production, *Geophys. Res. Lett.*, *35*(19), L19603.
654 Bauch, D., P. Schlosser, and R. G. Fairbanks (1995), Freshwater balance and the sources of
655 deep and bottom waters in the Arctic Ocean inferred from the distribution of $H_2{}^{18}O$,
656 *Progress In Oceanography*, *35*(1), 53-80.
657 Bauch, D., I. A. Dmitrenko, C. Wegner, J. Hölemann, S. A. Kirillov, L. A. Timokhov, and H.
658 Kassens (2009), Exchange of Laptev Sea and Arctic Ocean halocline waters in
659 response to atmospheric forcing, *J. Geophys. Res.*, *114*(C5), C05008.
660 Bauch, D., M. Rutgers van der Loeff, N. Andersen, S. Torres-Valdes, K. Bakker, E. P.
661 Abrahamsen (2011). Origin of freshwater and polynya water in the Arctic Ocean
662 halocline in summer 2007. *Progress in Oceanography*, 10.1016/j.pocean.2011.07.017,
663 in press
664 Boyd, P., A. Watson, C. Law, E. Abraham, T. Trull, R. Murdoch, D. Bakker, A. Bowie, K.
665 Buesseler, and H. Chang (2000), A mesoscale phytoplankton bloom in the polar
666 Southern Ocean stimulated by iron fertilization, *Nature*, *407*(6805), 695-702.
667 Boyle, E.A., J.M. Edmund, E.R. Sholkovitz (1977), The mechanism of iron removal in
668 estuaries. *Geochimica et Cosmochimica Acta* 41(9), 1313-1324.

669 Broecker, W. S., T. Takahashi, and T. Takahashi (1985), Sources and Flow Patterns of Deep-
670 Ocean Waters as Deduced From Potential Temperature, Salinity, and Initial Phosphate
671 Concentration, *J. Geophys. Res.*, *90*(C4), 6925-6939.
672 Cai, P., M. Rutgers van der Loeff, I. Stimac, E. M. Nöthig, K. Lepore, and S. B. Moran
673 (2010), Low export flux of particulate organic carbon in the central Arctic Ocean as
674 revealed by 234Th:238U disequilibrium, *J. Geophys. Res.*, *115*(C10), C10037.
675 Cámara-Mor, P., P. Masqué, J. Garcia-Orellana, J. K. Cochran, J. L. Mas, E. Chamizo, and C.
676 Hanfland (2010), Arctic Ocean sea ice drift origin derived from artificial
677 radionuclides, *Science of The Total Environment*, *408*(16), 3349-3358.
678 Carmack, E., and P. Wassmann (2006), Food webs and physical-biological coupling on pan-
679 Arctic shelves: Unifying concepts and comprehensive perspectives, *Progress In*
680 *Oceanography*, *71*(2-4), 446-477.
681 Codispoti, L. A., C. Flagg, V. Kelly, and J. H. Swift (2005), Hydrographic conditions during
682 the 2002 SBI process experiments, *Deep Sea Research Part II: Topical Studies in*
683 *Oceanography*, *52*(24-26), 3199-3226.
684 Cooper, L.W., J.W. McClelland, R.M. Holmes, P.A. Raymond, J.J. Gibson, C.K. Guay, B.J.
685 Peterson (2008), Flow-weighted values of runoff tracers (d18O, DOC, Ba, alkalinity)
686 from the six largest Arctic rivers, *Geophysical Research Letters* 35,
687 doi:10.1029/2008GL035007
688 Craig, H. (1961), Isotopic variations in meteoric waters, *Science (133),* 1702-1703.
689 Dai, M.-H., and J.-M. Martin (1995), First data on trace metal level and behaviour in two
690 major Arctic river-estuarine systems (Ob and Yenisey) and in the adjacent Kara Sea,
691 Russia, *Earth and Planetary Science Letters*, *131*(3-4), 127-141.
692 Dickson, A.,2001. Reference material for oceanic CO_2 measurements. Oceanography 14,21-
693 22.

694 Dickson, A.G., C.L. Sabine, J. Christian (2007), Guide to best practices for ocean CO_2
695 measurements. PICES Special Publication 3, 191 pp.
696 Darby, D. A., L. H. Burckle, and D. L. Clark (1974), Airborne dust on the Arctic pack ice, its
697 composition and fallout rate, *Earth and Planetary Science Letters*, *24*(2), 166-172.
698 de Baar, H. J. W., J. T. M. de Jong, D. C. E. Bakker, B. M. Loscher, C. Veth, U. Bathmann,
699 and V. Smetacek (1995), Importance of iron for plankton blooms and carbon dioxide
700 drawdown in the Southern Ocean, *Nature*, *373*(6513), 412-415.
701 de Baar, H.J.W, K.R. Timmermans, P. Laan, P., H. H. De Porto, Ober, S., J.J. Blom, M. C.
702 Bakker, J. Schilling, G. Sarthou, M.G. Smit and M. Klunder (2008), Titan: a new
703 facility for ultraclean sampling of trace elements and isotopes in the interantional
704 Geotraces program, *Marine Chemistry*, 111(1-2),4-21
705 Ekwurzel, B., P. Schlosser, R. A. Mortlock, R. G. Fairbanks, and J. H. Swift (2001), River
706 runoff, sea-ice meltwater, and Pacific water distribution and mean residence times in
707 the Arctic Ocean, *J. Geophys. Res.*, *106*(C5), 9075-9092.
708 Feldman, G. C., C. R. McClain, Ocean Color Web, SEAWifs 4,NASA Goddard Space Flight
709 Center. Eds. N. Kuring, S.W. Bailey, 27-01-2011. http://oceancolor.gsfc.nasa.gov/
710 Falkowski, P.G., Barber, R.T., Smetacek, V., 1998. Biogeochemical controls and feedbacks in
711 Ocean Primary production. *Science*, 281 (200).
712 Gebhardt, A. C., F. Schoster, B. Gaye-Haake, B. Beeskow, V. Rachold, D. Unger, and V.
713 Ittekkot (2005), The turbidity maximum zone of the Yenisei River (Siberia) and its
714 impact on organic and inorganic proxies, *Estuarine, Coastal and Shelf Science*, *65*(1-
715 2), 61-73.
716 Gosselin, M., M. Levasseur, P. A. Wheeler, R. A. Horner, and B. C. Booth (1997), New
717 measurements of phytoplankton and ice algal production in the Arctic Ocean, *Deep*
718 *Sea Research Part II: Topical Studies in Oceanography*, *44*(8), 1623-1644.

719 Guay, C. K., and K. Kenison Falkner (1997), Barium as a tracer of Arctic halocline and river
720 waters, *Deep Sea Research Part II: Topical Studies in Oceanography*, *44*(8), 1543-
721 1569.
722 Guay, C. K. H., F. A. McLaughlin, and M. Yamamoto-Kawai (2009), Differentiating fluvial
723 components of upper Canada Basin waters on the basis of measurements of dissolved
724 barium combined with other physical and chemical tracers, *J. Geophys. Res.*, *114*(C1),
725 C00A09.
726 Harms, I. H., M. J. Karcher, and D. Dethleff (2000), Modelling Siberian river runoff --
727 implications for contaminant transport in the Arctic Ocean, *Journal of Marine*
728 *Systems*, *27*(1-3), 95-115.
729 Hölemann, J. A., M. Schirmacher, and A. Prange (2005), Seasonal variability of trace metals
730 in the Lena River and the southeastern Laptev Sea: Impact of the spring freshet,
731 *Global and Planetary Change*, *48*(1-3), 112-125.
732 Holmes, R.M., J.W. McClelland, B.J. Peterson, I.A. Shiklomanov, A.I. Shiklomanov, A. V.
733 Zhulidov, V.V. Gordeev, N. N. Bobrovitskaya (2002), A circumpolar perspective on
734 fluvial sediment flux to the Arctic Ocean. *Glob. Biogeochem. Cycl.* 16 (4) 1098,
735 doi:10.1029/2001GB001849
736 Johnson, K. S., R. M. Gordon, and K. H. Coale (1997), What controls dissolved iron
737 concentrations in the world ocean?, *Marine Chemistry*, *57*(3-4), 137-161.
738 Jones, E.P., L.G. Anderson and J.H. Swift, (1998) Distribution of Atlantic and Pacific waters
739 in the upper Arctic Ocean : Implications for circulation. *Geophys. Res. Lett .*, *25(6),*
740 765-768.

741 Jones, E.P., L. G. Anderson, S. Jutterström, L. Mintrop, and J. H. Swift (2008), Pacific
742 freshwater, river water and sea ice meltwater across Arctic Ocean basins: Results from

743 the 2005 Beringia Expedition , *J. Geophys. Res.* , 113 , C08012,
744 doi:10.1029/2007JC004124.

745 Klunder, M. B., P. Laan, R. Middag, H. J. W. De Baar, and J. v. Ooijen (2010), Dissolved
746 iron in the Southern Ocean (Atlantic sector), *Deep Sea Research Part II: Topical*
747 *Studies in Oceanography*, *available online.*

748 Klunder, M.B., P. Laan,R. Middag and H.J.W. De Baar, Dissolved Fe in the Arctic Ocean:
749 important role of hydrothermal sources, shelf input and scavenging removal, *accepted*
750 *for publication in Journal of Geophysical Research, June 2011*.

751 Lannuzel, D., V. Schoemann, J. de Jong, L. Chou, B. Delille, S. Becquevort, and J.-L. Tison
752 (2008), Iron study during a time series in the western Weddell pack ice, *Marine*
753 *Chemistry*, *108*(1-2), 85-95.

754 Martin, J. H. and R. M. Gordon (1988), Northeast Pacific iron distributions in relation to
755 phytoplankton productivity, *Deep Sea Research Part A. Oceanographic Research*
756 *Papers*, *35*(2), 177-196.

757 Measures, C. I. (1999), The role of entrained sediments in sea ice in the distribution of
758 aluminium and iron in the surface waters of the Arctic Ocean, *Marine Chemistry*,
759 *68*(1-2), 59-70.

760 Middag, R., P. Laan, H.J.W. De Baar, M.B. Klunder (2011), Fluvial and hydrothermal input
761 of manganese into the Arctic Ocean, *Geochimica et Cosmochimica Acta, available*
762 *online*

763 Middag, R., H. J. W. de Baar, P. Laan, and K. Bakker (2009), Dissolved aluminium and the
764 silicon cycle in the Arctic Ocean, *Marine Chemistry*, *115*(3-4), 176-195.

765 Moore, R.M. (1983), The relationship between distributions of dissolved cadmium, iron and
766 aluminium and hydrography in the central Arctic Ocean. In C.S. Wong, E. Boyle,

767 K.W. Bruland, J.S. Burton and E.D. Goldberg (Eds.), Trace metals in Sea Water,
768 Plenum Press, New York, pp. 131-142.
769 Moore, J. K., and O. Braucher (2008), Sedimentary and mineral dust sources of dissolved iron
770 to the world ocean, *Biogeosciences*, *5*(3), 631-656.
771 Nürnberg, D., I. Wollenburg, D. Dethleff, H. Eicken, H. Kassens, T. Letzig, E. Reimnitz, and
772 J. Thiede (1994), Sediments in Arctic sea ice: implications for entrainment, transport
773 and release, *Marine Geology*, *119*(3-4), 185-214.
774 Östlund, H. G., and G. Hut (1984), Arctic Ocean Water Mass Balance From Isotope Data, *J.*
775 *Geophys. Res.*, *89*(C4), 6373-6381.
776 Pabi, S., G. L. van Dijken, and K. R. Arrigo (2008), Primary production in the Arctic Ocean,
777 1998-2006, *J. Geophys. Res.*, *113*(C8), C08005.
778 Rintoul, S., C. W. Hughes, and D. Olbers (2001), Chapter 4.6 The antarctic circumpolar
779 current system, in *International Geophysics*, edited by J. C. Gerold Siedler and G.
780 John, pp. 271-302, XXIX-XXXVI, Academic Press.
781 Rember, R. D., and J. H. Trefry (2004), Increased concentrations of dissolved trace metals
782 and organic carbon during snowmelt in rivers of the alaskan arctic, *Geochimica et*
783 *Cosmochimica Acta*, *68*(3), 477-489.
784 Roeske, T., Rutgers van der Loeff, M., D. Bauch. Utility of dissolved Ba in distinguishing
785 North American from Eurasian runoff and in the light of its part in biogeochemical
786 cycling of the Arctic Ocean, *manuscript in preparation (note for reviewers: this is part*
787 *of thesis work of T. Roeske, and will be submitted soon).*
788 Rudels, B., E. P. Jones, U. Schauer, and P. Eriksson (2004), Atlantic sources of the Arctic
789 Ocean surface and halocline waters, *Polar Research*, *23*(2), 181-208.
790 Rudels, B. (2001), Ocean Current: Arctic Basin Circulation. In "Encyclopedia of Ocean
791 Sciences" Eds J. Steele, S. Thorpe and K. Turekian. Academic Press, 177-187.

792 Rutgers van der Loeff, M., O. Cai, I. Stimac, D. Bauch, C. Hanfland, T. Roeske and B. Moran
793 (Submitted), Shelf-basin exchange times of Arctic surface waters estimated from
794 228^{Th}/228Ra disequilibrium. Submitted to JGR Oceans, August 2011.
795 Serreze, M.P, A. P. Barrett, A. G. Slater, R.A. Woodgate, K. Aagaard, R.B. Lammers, M.
796 Steele, R. M., M. Meredith, and C.M. Lee (2006), The large-scale freshwater cycle of
797 the Arctic. *J. Geophys. Res.*, 111 (C11), C11010.
798 Sedwick and DiTullio (1997), Regulation of algal blooms in Antarctic Shelf waters by the
799 release of iron from melting sea ice. *Geophys. Res. Letters* 24 (20), 2515-2518.
800 Spreen, G. and L. Kaleschke (2008), AMSR-E ASI 6.25 km Sea-Ice Concentration Data
801 V5.4. Institute of Oceanography, University of Hamburg, Germany, digital media
802 (ftp.projects.zmaw.de/sea-ice)
803 Steele, M., T. Boyd (1998), retreat of the cold halocline layer in the Arctic Ocean. *J. Geophys.*
804 *Res.*, 103 (C5).
805 Takata, H.,K. Kuma, S. Iwade, Y. Yamajyoh, A. Yamaguchi., S. Takagi., K. Sakaoka, Y.
806 Yasahit, E. Tanoue, T. Midorikawa, K. Kimura and J. Nishioka. (2004), Spatial
807 variability of iron in the surface water of the northwestern North Pacific Ocean,
808 *Marine Chemistry*, *86*(3-4), 139-157.
809 Thuroczy, C.E.T, L.J.A. Gerringa, M.B. Klunder, P.Laan, H.J.W. De Baar, Distinct trends in
810 the iron speciation between the shallow shelf seas and the deep basins of the Arctic
811 Ocean. *Journal of Geophysical Research – Oceans*, In Press August 2011.
812 Tovar-Sanchez, A., C. M. Duarte, S. Hernández-León, and S. A. Sañudo-Wilhelmy (2009),
813 Impact of submarine hydrothermal vents on the metal composition of krill and its
814 excretion products, *Marine Chemistry*, *113*(1-2), 129-136.
815 van der Merwe, P., D. Lannuzel, C. A. M. Nichols, K. Meiners, P. Heil, L. Norman, D. N.
816 Thomas, and A. R. Bowie (2009), Biogeochemical observations during the winter-

817 spring transition in East Antarctic sea ice: Evidence of iron and exopolysaccharide
818 controls, *Marine Chemistry*, *115*(3-4), 163-175.
819 Woodgate, R. A., K. Aagaard, and T. J. Weingartner (2005), A year in the physical
820 oceanography of the Chukchi Sea: Moored measurements from autumn 1990-1991,
821 *Deep Sea Research Part II: Topical Studies in Oceanography*, *52*(24-26), 3116-3149.
822 Yamamoto-Kawai, M., N. Tanaka, and S. Pivovarov (2005), Freshwater and brine behaviors
823 in the Arctic Ocean deduced from historical data of $\delta^{18}O$ and alkalinity (1929-2002
824 A.D.), *J. Geophys. Res.*, *110*(C10), C10003.
825 Yamamoto-Kawai, M., E. Carmack, and F. McLaughlin (2006), Nitrogen balance and Arctic
826 throughflow, *Nature*, *443*(7107), 43-43.
827 Yamamoto-Kawai, M., F. A. McLaughlin, E. C. Carmack, S. Nishino, and K. Shimada
828 (2008), Freshwater budget of the Canada Basin, Arctic Ocean, from salinity, $\delta^{18}O$, and
829 nutrients , *J. Geophys. Res.* , 113 , C01007, doi:10.1029/2006JC003858.
830
831
832 **9. Figure captions**
833
834 Fig. 1a. Station map of all stations occupied during ARK XXII/2. Color scale indicates
835 dissolved Fe averages of Surface Layer Waters (SLW). Stations measured for total Fe (TFe)
836 are marked with an open diamond ◊. Average salinity isolines of the Surface Layer Waters are
837 shown in red. Blue arrows indicate the transpolar drift (schematically, after Rudels et al.
838 [2001]). Abbreviations: NB: Nansen Basin; AB: Amundsen Basin; MB: Makarov Basin.
839
840 Fig. 1b. Map of the Arctic Ocean, with the transects and shelf stations occupied during ARK
841 XXII/2. The grey square in the overview marks the position of the enlargement (right panel)

for the Arctic shelves. Abbreviations: BS: Barents Sea; FJL: Franz Josef Land; BS: Barents Sea; KS: Kara Sea; LS: Laptev Sea; NB: Nansen Basin; GR: Gakkel Ridge; AB: Amundsen Basin; LR; Lomonosov Ridge; MB: Makarov Basin; MR: Mendeleev Ridge.

Fig 2. Depth profiles of DFe, Salinity and fluorescence (indicative of Chl-a; arbitrary units) for the stations on (a) the Barents Sea Shelf, (b) Kara Sea Shelf and (c) the Laptev Sea Shelf (see Fig. 1b). For clarification of the discussion, for the Kara Sea shelf, also oxygen profiles are shown (see text) and for the Laptev Sea shelf also light transmission data is shown (see text). Station profiles for salinity, fluorescence, light transmission and oxygen follow the same colors as indicated in the DFe profile for each region.

Fig. 3. Dissolved Fe depth profiles, dissolved Fe transect plot (upper panel) and transect plot of river water fractions (color) and sea-ice meltwater fractions (contours) (lower panel) in the upper 250 m of the water column at transect 1 (see Fig. 1b). Station numbers of transects are indicated above upper panel and South (S) and North (N) orientation within lower panel. Note the different scale for the DFe depth profiles. [Gridding: DIVA gridding (ODV) ; 72*72 (upper panel)& 60*60 (lower panel)]

Fig 4. Dissolved Fe depth profiles, dissolved Fe transect plot (upper panel) and transect plot of river water fractions (color) and sea-ice meltwater fractions (contours) (lower panel) in the upper 250 m of the water column at transect 2 (see Fig. 1b). Station numbers of transects are indicated above upper panel and South (S) and North (N) orientation within lower panel. Note the different scale for the DFe depth profiles. [Gridding: DIVA gridding (ODV); 90*90 (upper panel)& 60*60 (lower panel)]

867 Fig. 5. Dissolved Fe depth profiles, dissolved Fe transect plot (upper panel) and transect plot
868 of river water fractions (color) and sea-ice meltwater fractions (contours) (lower panel) in the
869 upper 250 m of the water column at transect 3/4 (see Fig. 1b). Station numbers of transects are
870 indicated above upper panel and South (S) and North (N) orientation within lower panel. The
871 different Basins are indicated by arrows below the transect plots. Note the different scale for
872 the DFe depth profiles. The red bar in the lower panel indicates the region where water mass
873 fractions are calculated using N/P ratio. [Gridding: DIVA gridding (ODV); 72*72 (upper
874 panel)& 60*60 (lower panel)]
875
876 Fig. 6. Dissolved Fe depth profiles, dissolved Fe transect plot (upper panel) and transect plot
877 of river water fractions (color) and sea-ice meltwater fractions (contours) (lower panel) in the
878 upper 250 m of the water column at transect 5 (see Fig. 1b). Station numbers of transects are
879 indicated above upper panel and South (S) and North (N) orientation within lower panel. Note
880 the different scale for the DFe depth profiles. [Gridding: DIVA gridding (ODV); 72*72
881 (upper panel)& 60*60 (lower panel)]
882
883 Fig. 7. Dissolved Fe datapoints plot (upper panel) and transect plot of of river water fractions
884 (color) and sea-ice meltwater fractions (contours) (lower panel) in the upper 250 m of the
885 water column of the stations on the Laptev Shelf (see Fig. 1b). Station numbers of transects
886 are indicated above upper panel and South (S) and North (N) orientation within lower panel.
887 [Gridding: DIVA gridding (ODV); 60*60 (lower panel)]
888
889 Fig 8a. Relation between DFe and Salinity in the upper 250 m. Red dots show all data,
890 (smaller) black dots show all data points excluding stations 338/342 (see text section 5.4) and

407/411 (see text section 5.2). Correlation coefficient, p-value and N are given for the reduced dataset (black dots). Note the break within the DFe axis.

Fig. 8b. Relation between the concentration of DFe (nM) and fraction of river water (%) for the whole water column in the Central Arctic Ocean (Shelf stations are excluded (Fig. 1b)). Fraction of Pacific-derived water (%) is shown in color scale. The blue ellipse indicates the data points >50 m at stations 338 and 342 (see text for discussion).

Fig. 9. Depth profiles in upper 300 m of DFe (nM), oxygen, salinity and salinity for stations 338 and 342 located on the North American side of the Transpolar Drift. Processes influencing the concentration of DFe are indicated (see text for explanation)

Fig. 10. Relation between Total Alkalinity and Salinity for the stations in the upper 250 m. DFe concentrations are shown in color. Mixing lines between Atlantic water and Eurasian (red dotted) and North American river water (red solid) and Pacific water and Eurasian (blue dotted) and North American river water (blue solid).
Endmember concentrations are following *Yamamoto-Kawaii et al.* [2005]; Salinity: Atlantic water: 34.87; Pacific Water 32.2 (mean of 32.7 [*Ekwurzel et al, 2001*] and 31.5 [*Anderson et al., 1994*]). Total Alkalinity: Atlantic water: 2306 µmol/kg and Pacific water: 2173 µmol/kg [*Anderson et al., 1994*]. The river endmembers are calculated using Sal=0 and alkalinity values of 1181, 845, 788, 1707, and 1540 µmol/kg for the Ob, Yenisey, Lena, Yukon, and Mackenzie Rivers, respectively **[***Cooper et al., 2008*] multiplied with the partial distribution of these rivers to the total endmember [*Holmes et al, 2002*].
Gray arrows indicate sea-ice melting and sea-ice formation, relative to the Atlantic – Eurasian river water mixing line. Green ellipse includes the data points at ~50 m in the TPD (stations 309 – 333 and 349 – 352) and orange ellipse indicates the waters at ~50 m north of the TPD. Laptev Sea data points (stat. 407 and 411) are surrounded by a blue square and are consistent with mixing with river water and a strong sea-ice formation/ brine input signal in the deepest layer of stat. 411 (see text section 5.2).

920 Fig. 11. Ratio total iron (TFe) over dissolved iron (DFe) for all points in the upper 100 m at
921 shelf stations (open circles) and open ocean stations (closed circles). Shelf Sea Stations are
922 indicated in Fig 1b.
923
924
925 **Supplementary Figures**
926
927 Fig. A 1a-d. SeaWifs Chlorophyll a images of the Barents Sea Region,of the months during
928 and prior to the ARK XXII/2 expedition.
929
930 Fig. A 2. Transect 1; Phosphate in color scale, DFe in contours.
931

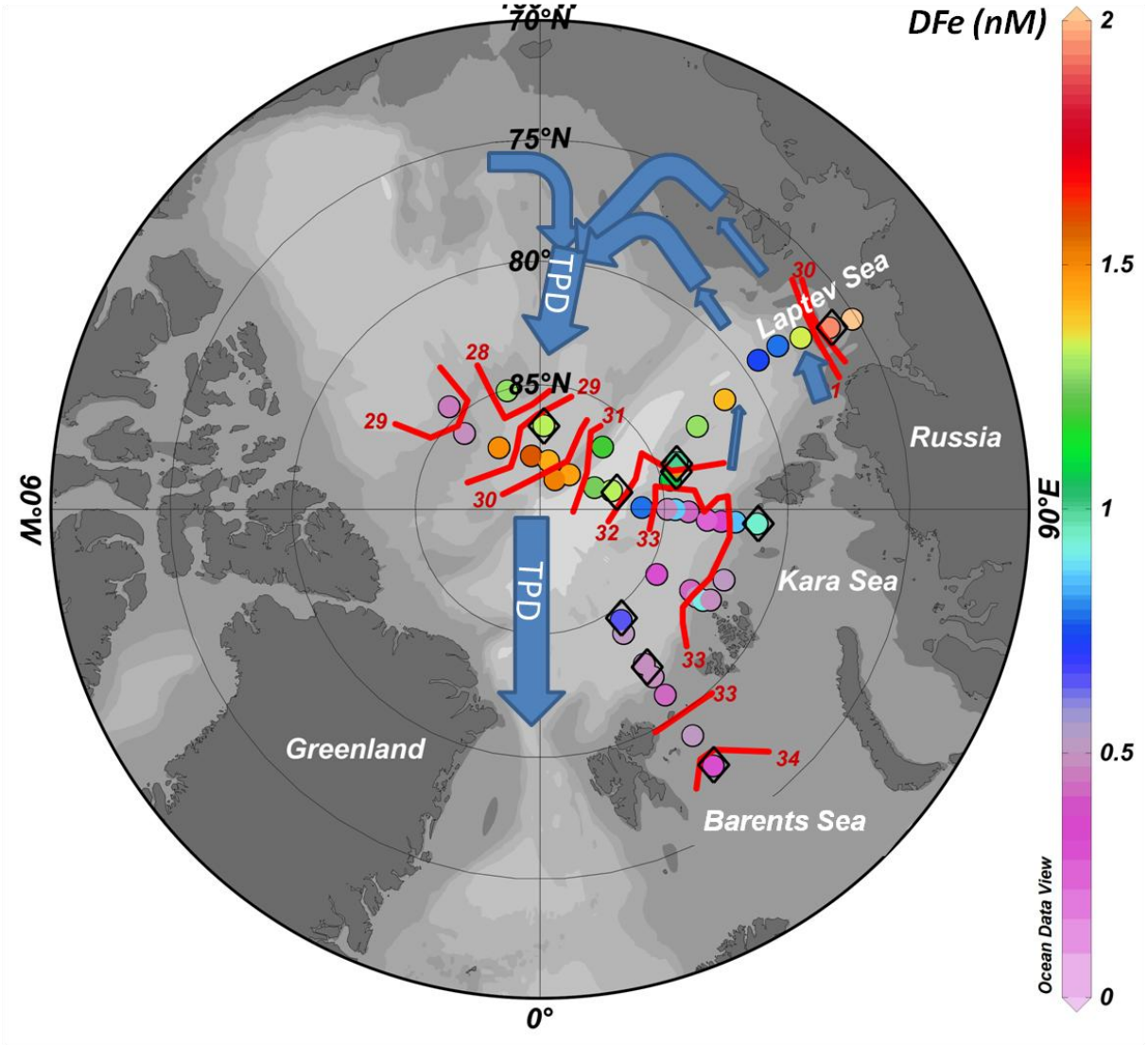

Fig. 1a. Station map of all stations occupied during ARK XXII/2. Color scale indicates dissolved Fe averages of Surface Layer Waters (SLW). Stations measured for total Fe (TFe) are marked with an open diamond ◊. Average salinity isolines of the Surface Layer Waters are shown in red. Blue arrows indicate the transpolar drift (schematically, after Rudels et al. [2001]). Abbreviations: NB: Nansen Basin; AB: Amundsen Basin; MB: Makarov Basin.

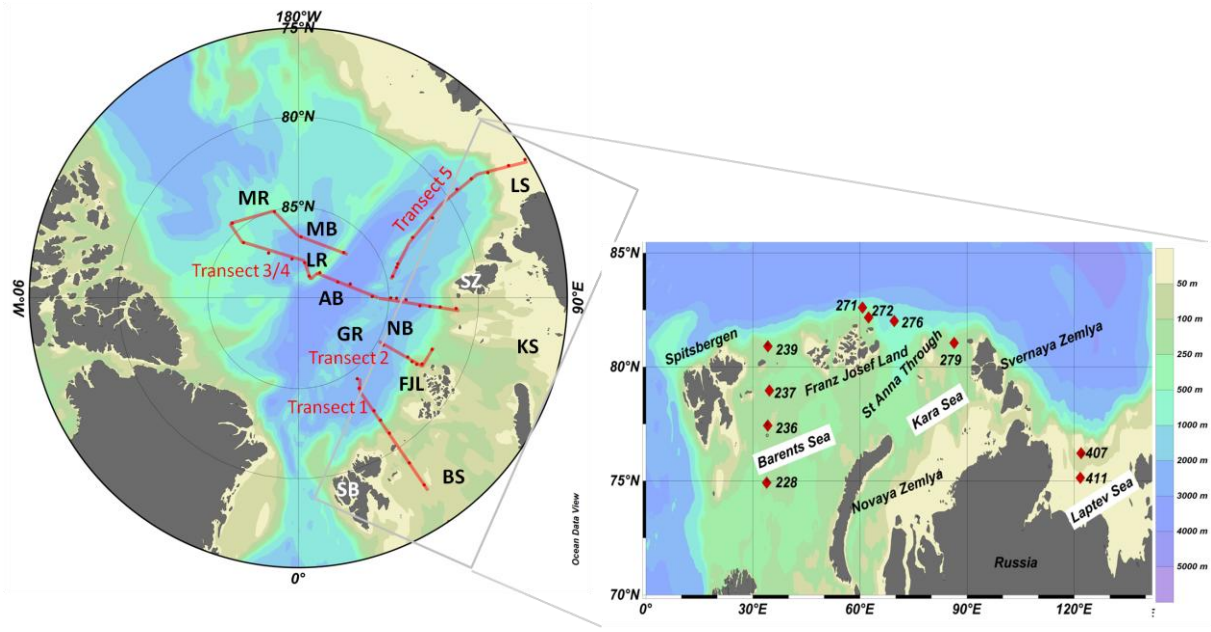

Fig. 1b. Map of the Arctic Ocean, with the transects and shelf stations occupied during ARK XXII/2. The grey square in the overview marks the position of the enlargement (right panel) for the Arctic shelves. Abbreviations: BS: Barents Sea; FJL: Franz Josef Land; BS: Barents Sea; KS: Kara Sea; LS: Laptev Sea; NB: Nansen Basin; GR: Gakkel Ridge; AB: Amundsen Basin; LR; Lomonosov Ridge; MB: Makarov Basin; MR: Mendeleev Ridge.

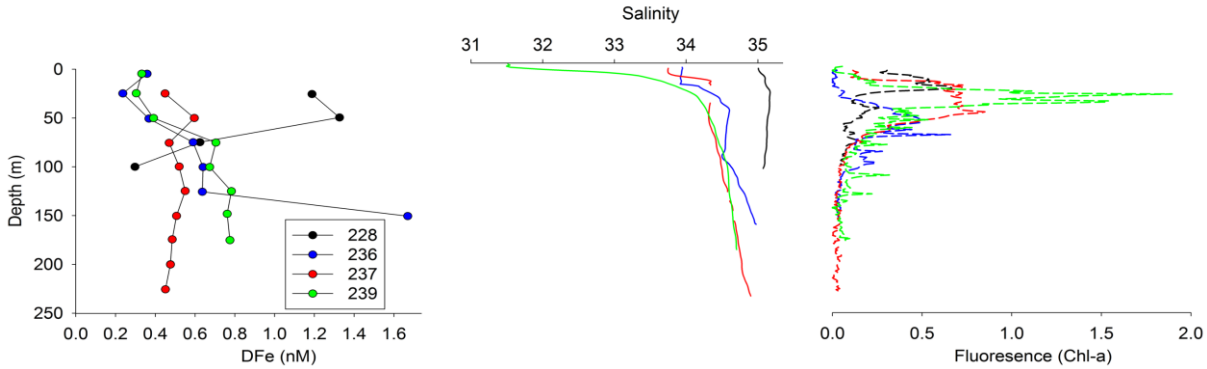

Fig. 2a

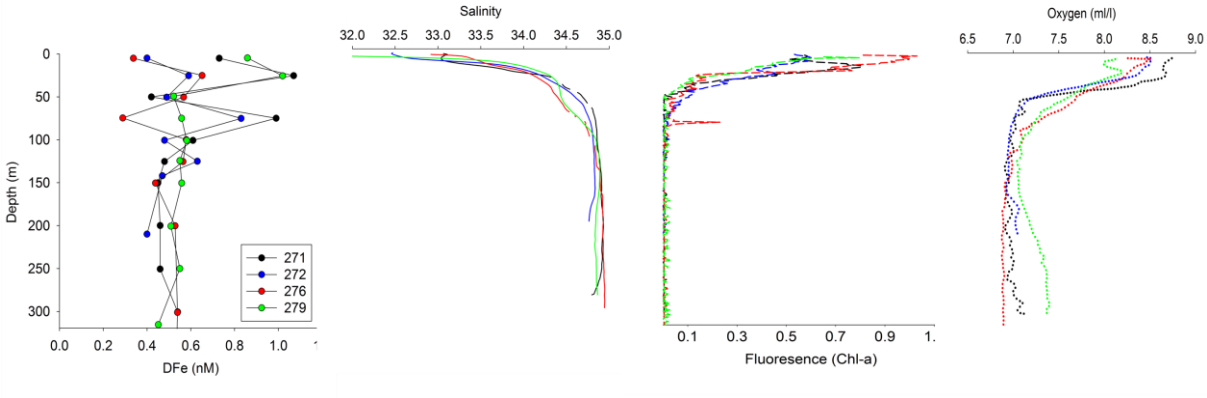

Fig. 2b

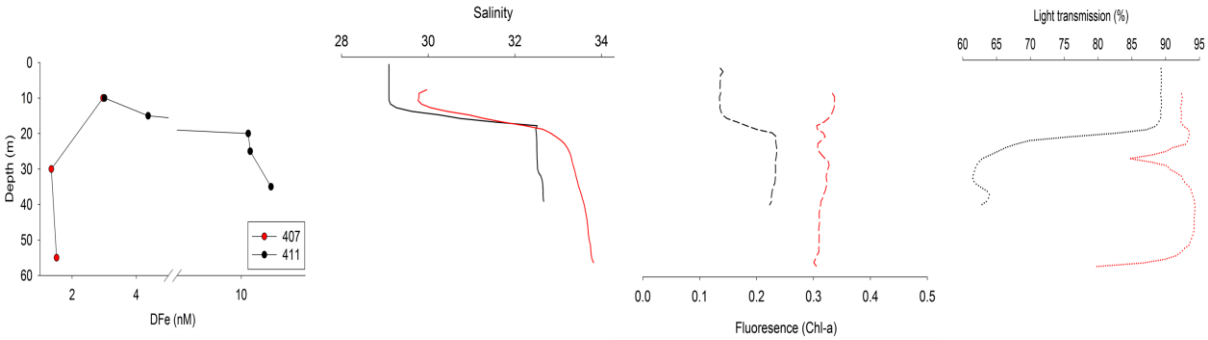

Fig 2c

Fig 2. Depth profiles of DFe, salinity and fluorescence (indicative of Chl-a; arbitrary units) for the stations on (a) the Barents Sea Shelf, (b) Kara Sea Shelf and (c) the Laptev Sea Shelf (see Fig. 1b). For clarification of the discussion, for the Kara Sea shelf, also oxygen profiles are shown (see text) and for the Laptev Sea shelf also light transmission data is shown (see text). Station profiles for salinity, fluorescence, light transmission and oxygen follow the same colors as indicated in the DFe profile for each region.

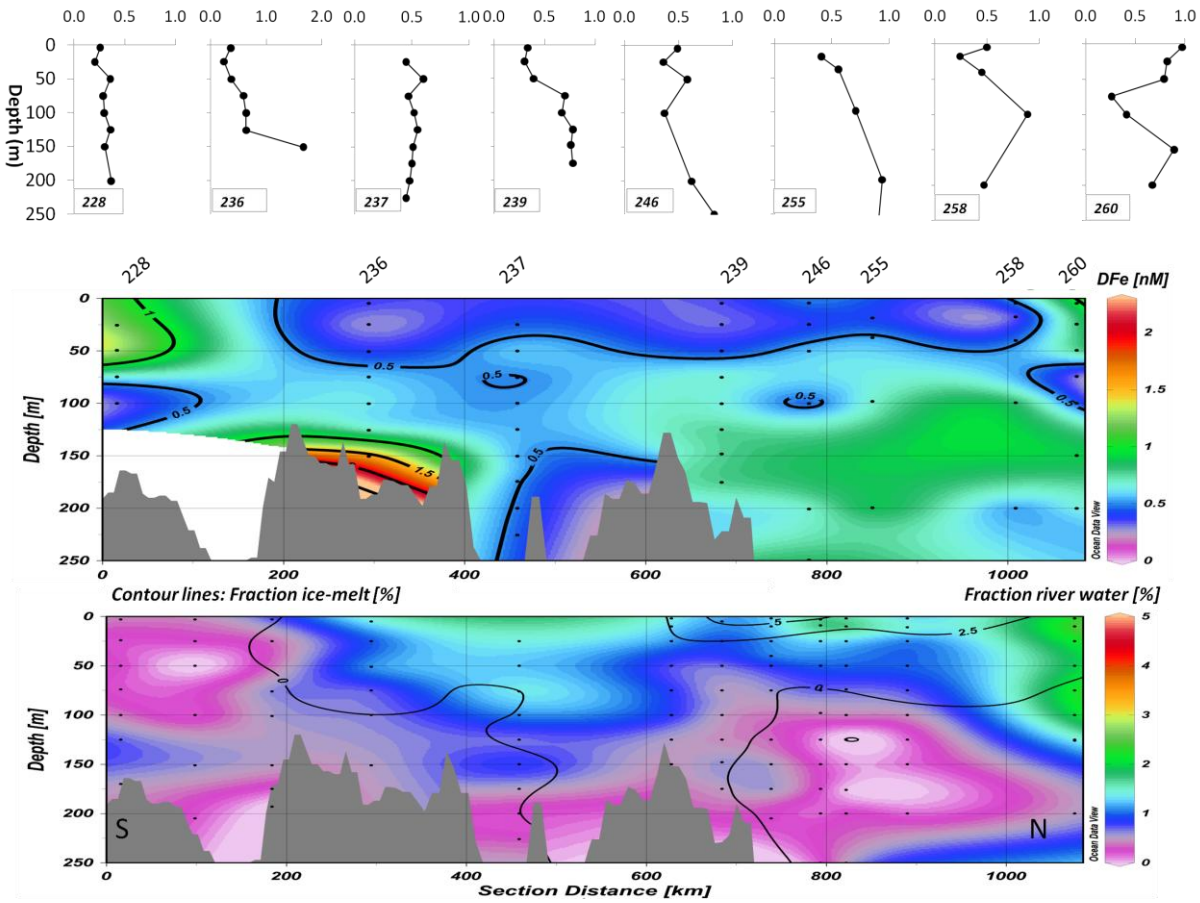

Fig. 3. Dissolved Fe depth profiles, dissolved Fe transect plot (upper panel) and transect plot of river water fractions (color) and sea-ice meltwater fractions (contours) (lower panel) in the upper 250 m of the water column at transect 1 (see Fig. 1b). Station numbers of transects are indicated above upper panel and South (S) and North (N) orientation within lower panel. Note the different scale for the DFe depth profiles. [Gridding: DIVA gridding (ODV) ; 72*72 (upper panel)& 60*60 (lower panel)].

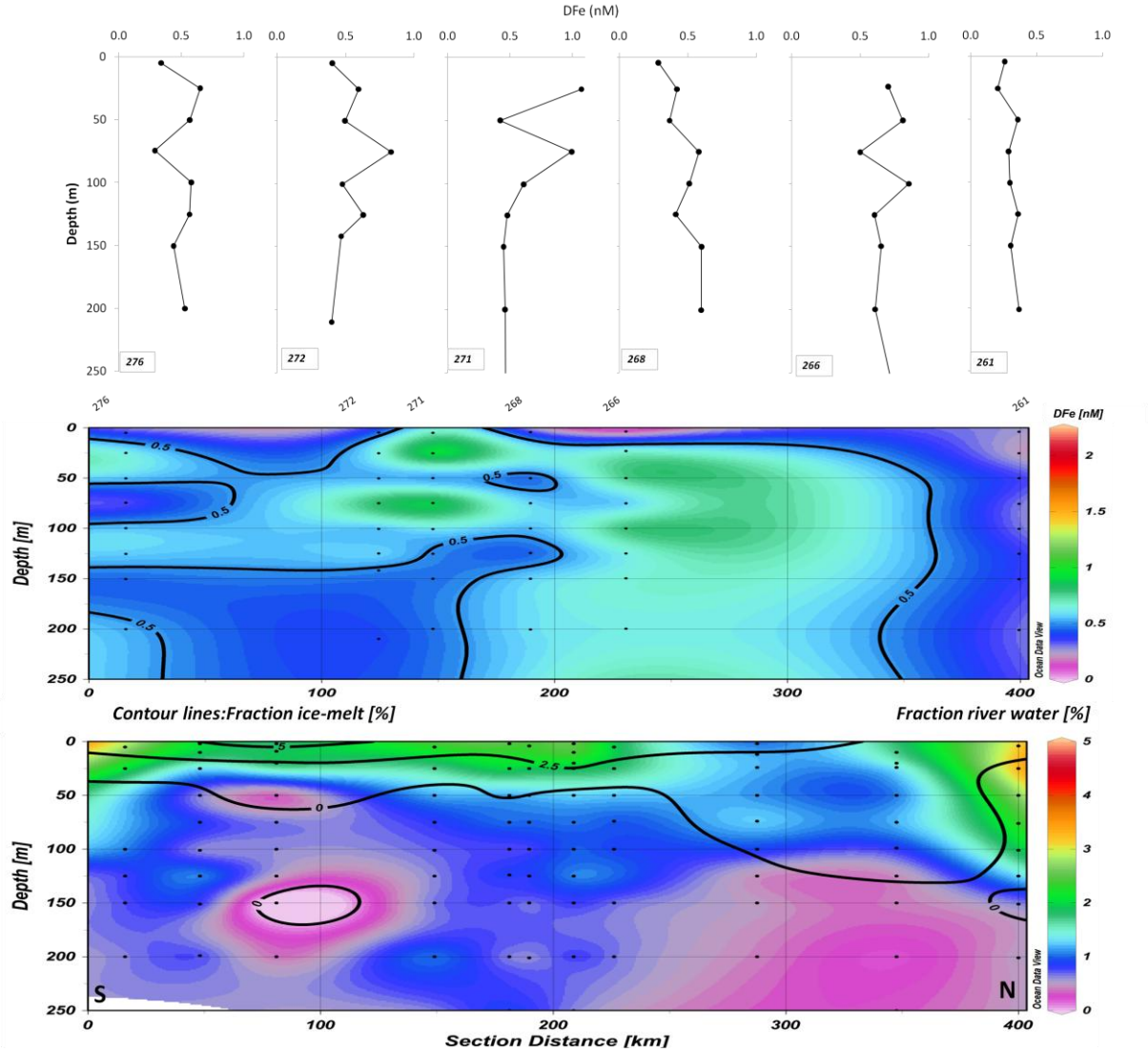

Fig 4. Dissolved Fe depth profiles, dissolved Fe transect plot (upper panel) and transect plot of river water fractions (color) and sea-ice meltwater fractions (contours) (lower panel) in the upper 250 m of the water column at transect 2 (see Fig. 1b). Station numbers of transects are indicated above upper panel and South (S) and North (N) orientation within lower panel. Note the different scale for the DFe depth profiles. [Gridding: DIVA gridding (ODV); 90*90 (upper panel)& 60*60 (lower panel)].

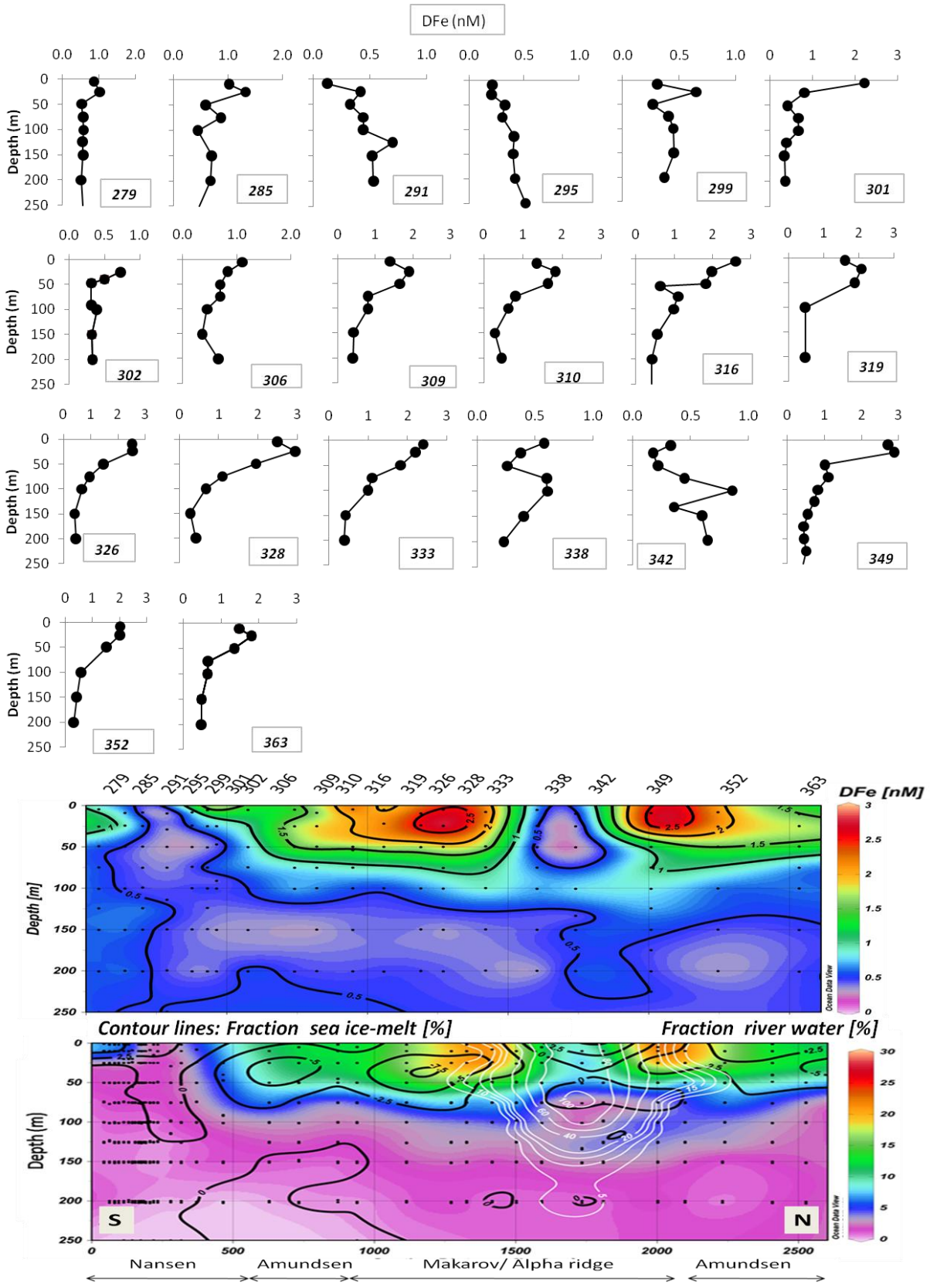
DFe (nM)
Depth (m)
279
285
291
295
299
301
302
306
309
310
316
319
326
328
333
338
342
349
352
363
DFe [nM]
Depth [m]
Contour lines: Fraction sea ice-melt [%]
Fraction river water [%]
S
N
Nansen
Amundsen
Makarov/ Alpha ridge
Amundsen

Fig. 5. Dissolved Fe depth profiles, dissolved Fe transect plot (upper panel) and transect plot of river water fractions (color) and sea-ice meltwater fractions (contours) (lower panel) in the upper 250 m of the water column at transect 3/4 (see Fig. 1b). Station numbers of transects are indicated above upper panel and South (S) and North (N) orientation within lower panel. The different Basins are indicated by arrows below the transect plots. Note the different scale for the DFe depth profiles. The red bar in the lower panel indicates the region where water mass fractions are calculated using N/P ratio. [Gridding: DIVA gridding (ODV); 72*72 (upper panel)& 60*60 (lower panel)]

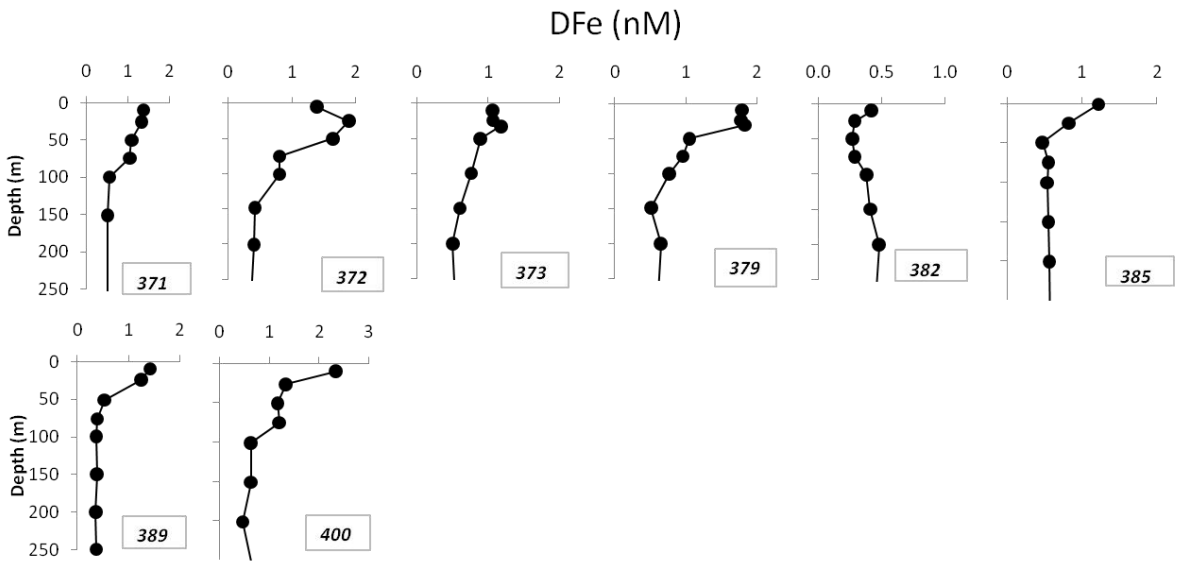
DFe (nM)
Depth (m)
371
372
373
379
382
385
389
400

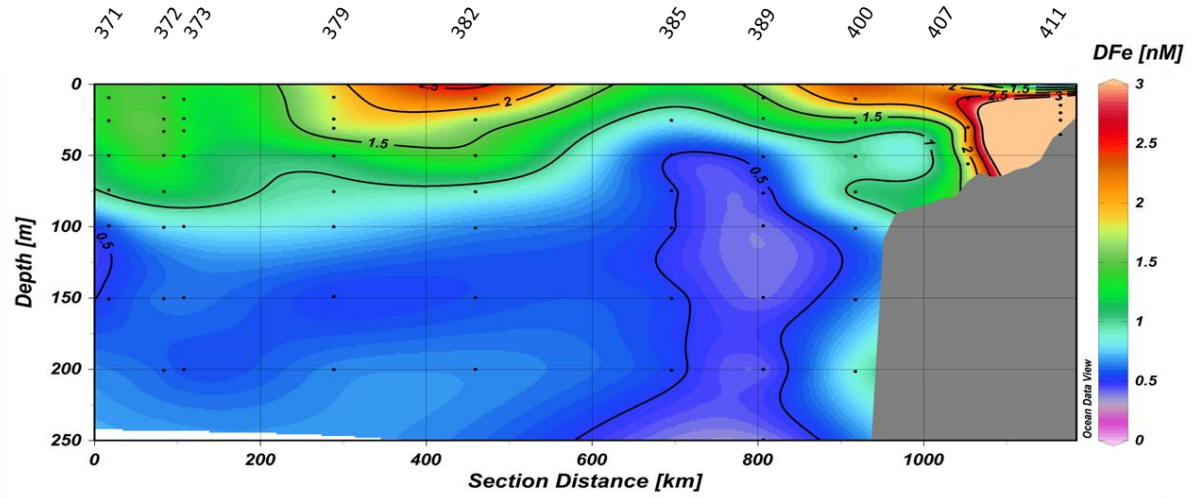
371
372
373
379
382
385
389
400
407
411
DFe [nM]
Depth [m]
Section Distance [km]
Ocean Data View

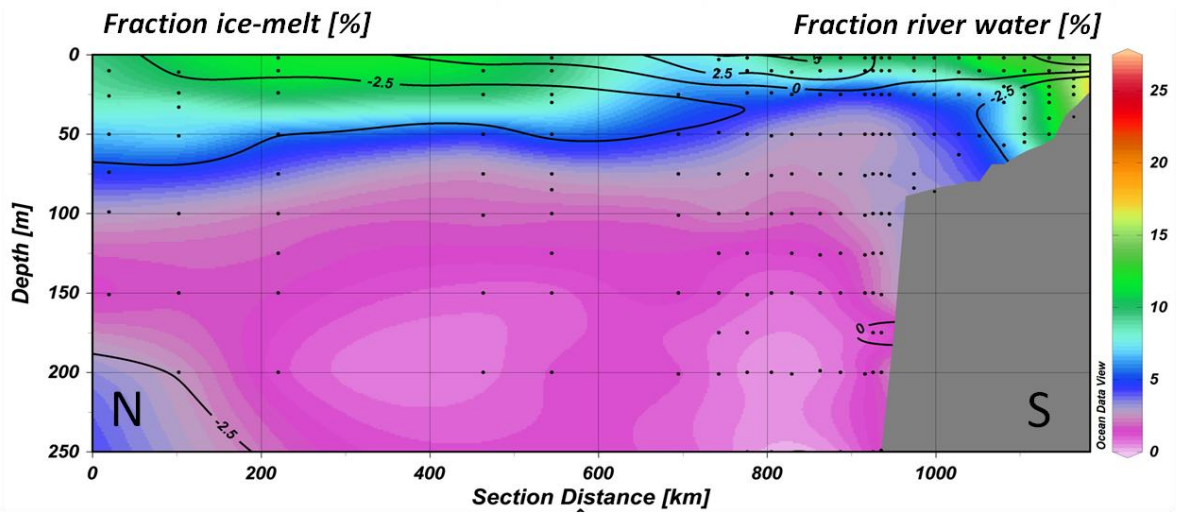
Fraction ice-melt [%]
Fraction river water [%]
Depth [m]
Section Distance [km]
N
S
Ocean Data View

Fig. 6. Dissolved Fe depth profiles, dissolved Fe transect plot (upper panel) and transect plot of river water fractions (color) and sea-ice meltwater fractions (contours) (lower panel) in the upper 250 m of the water column at transect 5 (see Fig. 1b). Station numbers of transects are indicated above upper panel and South (S) and North (N) orientation within lower panel. Note the different scale for the DFe depth profiles. [Gridding: DIVA gridding (ODV); 72*72 (upper panel)& 60*60 (lower panel)]

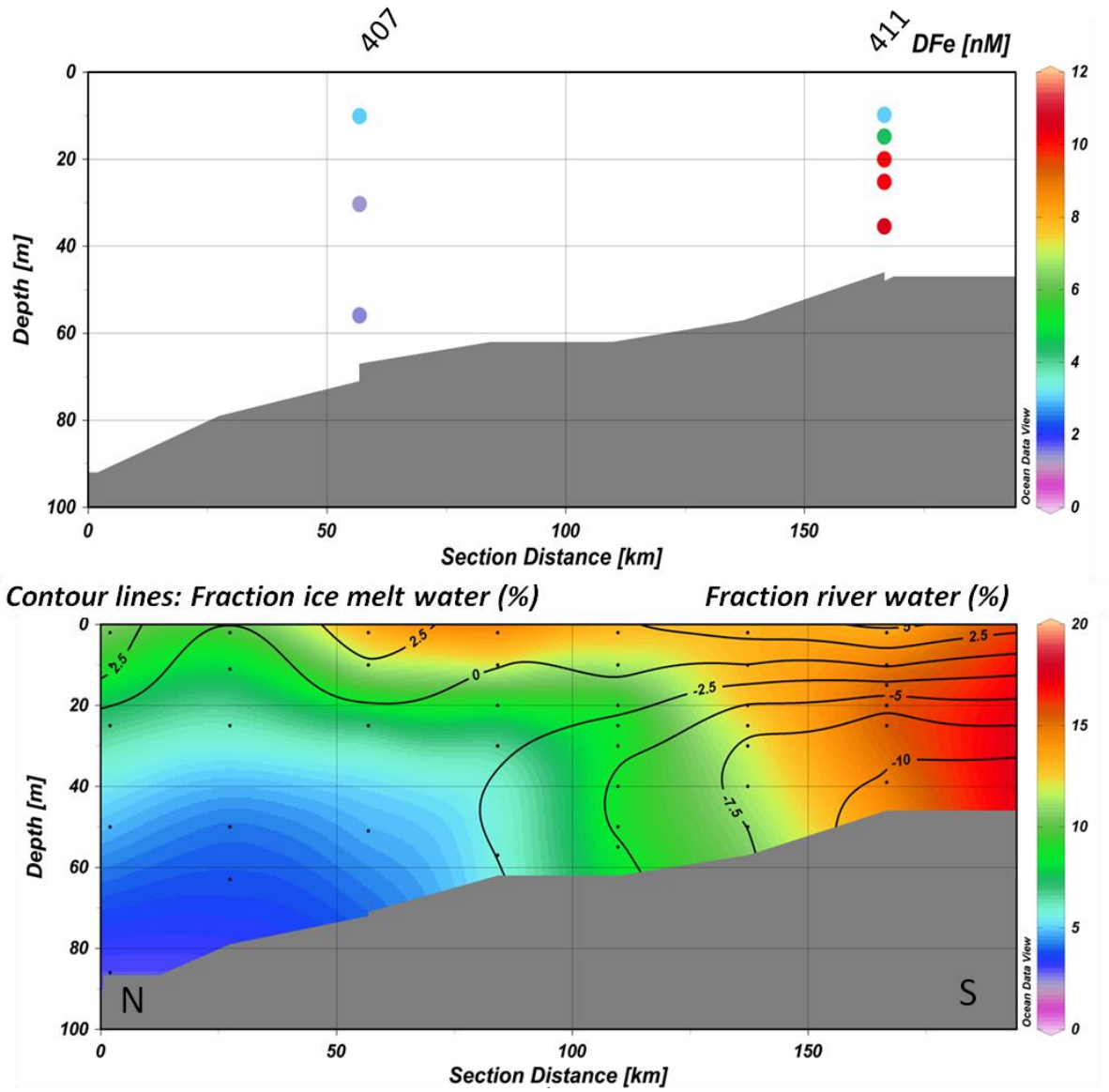

Fig. 7. Dissolved Fe datapoints plot (upper panel) and transect plot of of river water fractions (color) and sea-ice meltwater fractions (contours) (lower panel) in the upper 250 m of the water column of the stations on the Laptev Shelf (see Fig. 1b). Station numbers of transects are indicated above upper panel and South (S) and North (N) orientation within lower panel. [Gridding: DIVA gridding (ODV); 60*60 (lower panel)].

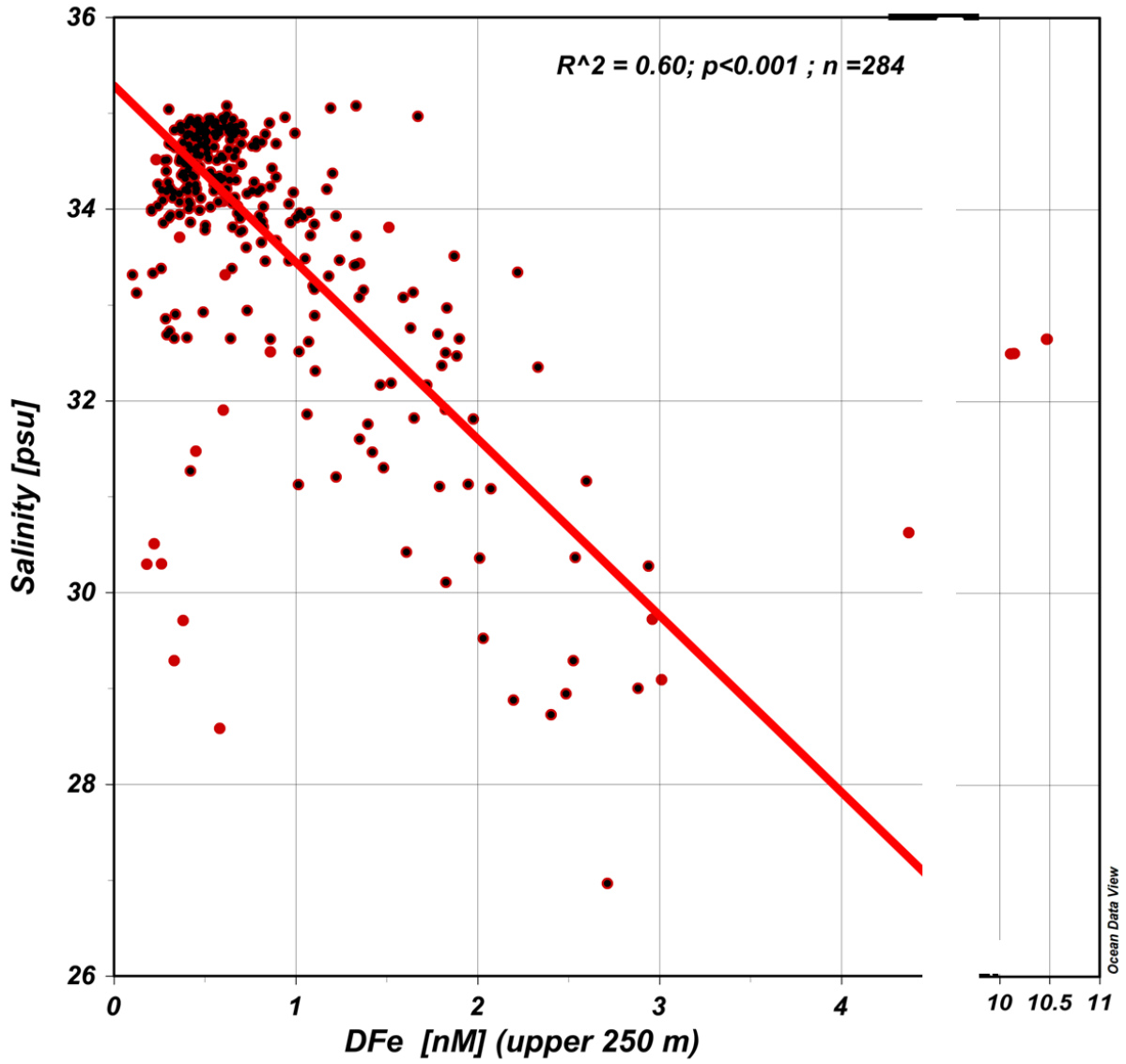

Fig 8a. Relation between DFe and Salinity in the upper 250 m. Red dots show all data, (smaller) black dots show all data points excluding stations 338/342 (see text section 5.4) and 407/411 (see text section 5.2). Correlation coefficient, p-value and N are given for the reduced dataset (black dots). Note the break within the DFe axis.

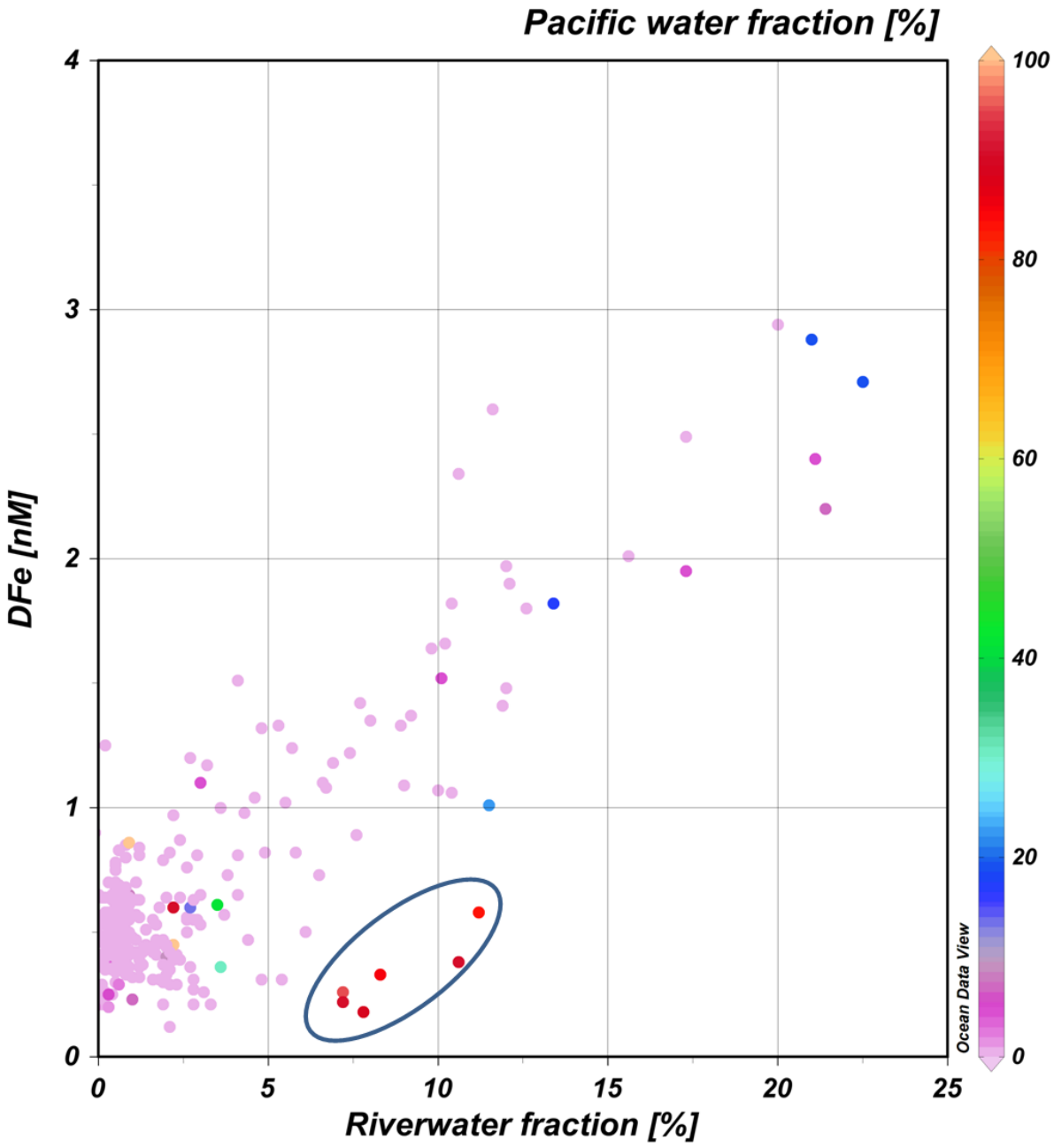

Fig. 8b. Relation between the concentration of DFe (nM) and fraction of river water (%) for the whole water column in the Central Arctic Ocean (Shelf stations are excluded (Fig. 1b)). Fraction of Pacific-derived water (%) is shown in color scale. The blue ellipse indicates the data points >50 m at stations 338 and 342 (see text for discussion).

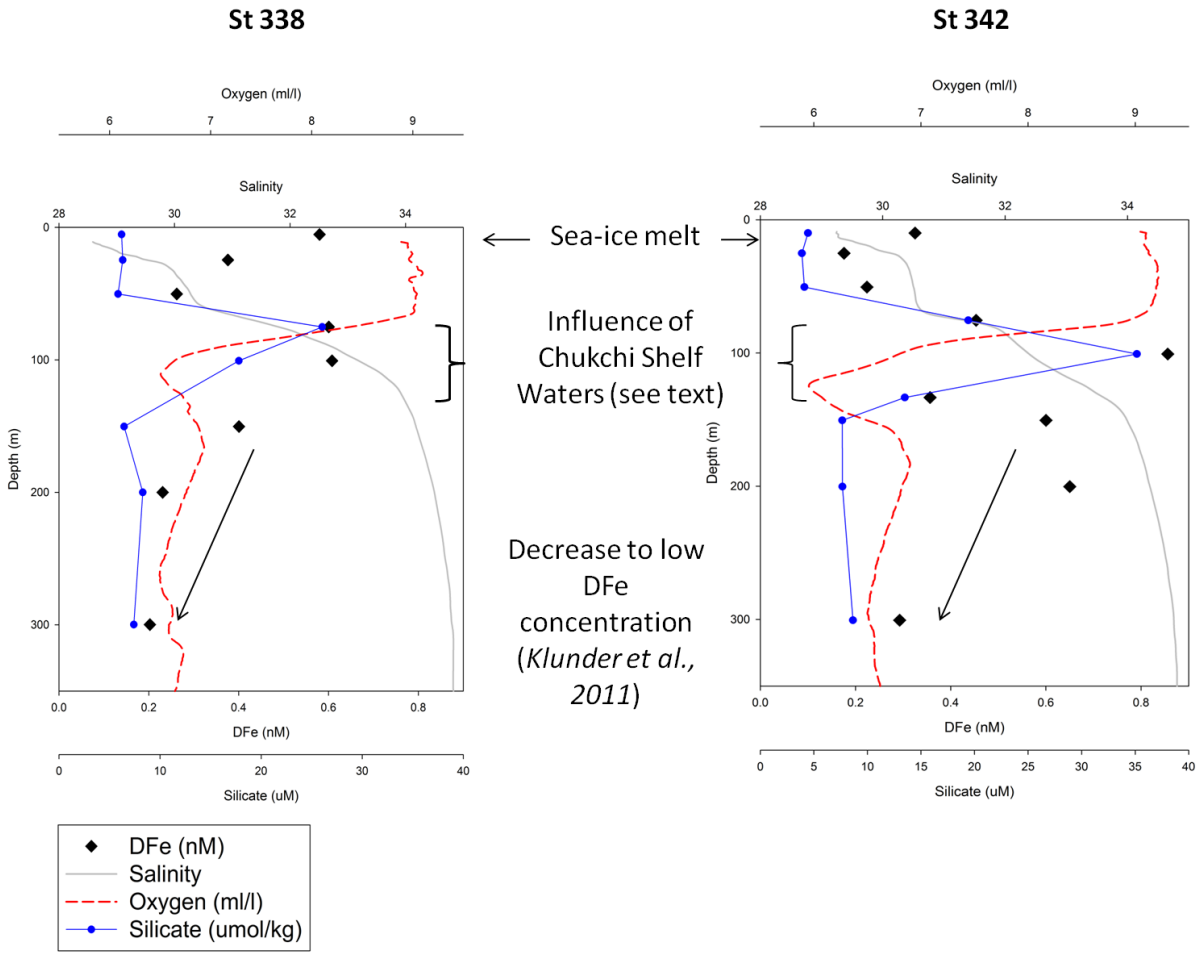

Fig. 9. Depth profiles in upper 300 m of DFe (nM), oxygen, salinity and salinity for stations 338 and 342 located on the North American side of the Transpolar Drift. Processes influencing the concentration of DFe are indicated (see text for explanation).

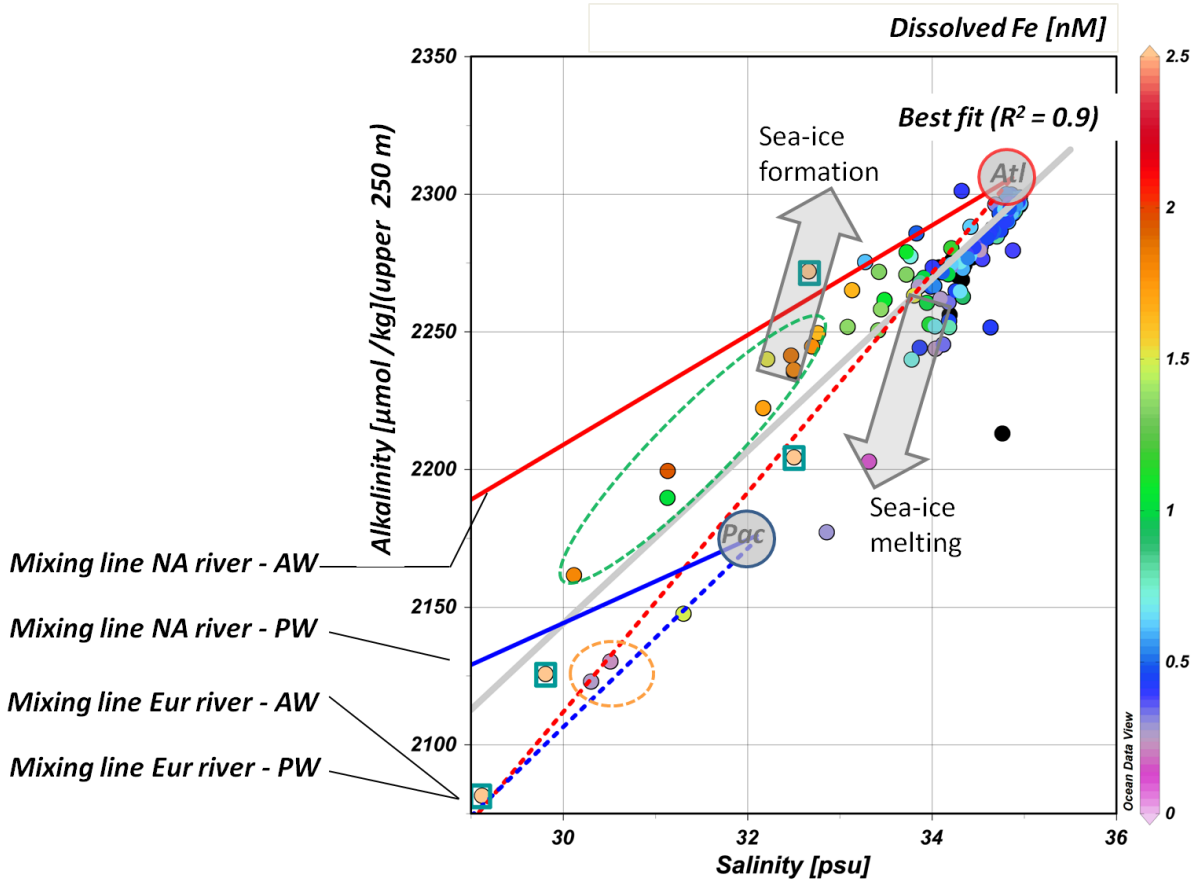

Fig. 10. Relation between Total Alkalinity and Salinity for the stations in the upper 250 m. DFe concentrations are shown in color. Mixing lines between Atlantic water and Eurasian (red dotted) and North American river water (red solid) and Pacific water and Eurasian (blue dotted) and North American river water (blue solid).

Endmember concentrations are following *Yamamoto-Kawaii et al.* [2005]; Salinity: Atlantic water: 34.87; Pacific Water 32.2 (mean of 32.7 [*Ekwurzel et al, 2001*] and 31.5 [*Anderson et al., 1994*]). Total Alkalinity: Atlantic water: 2306 µmol/kg and Pacific water: 2173 µmol/kg [*Anderson et al., 1994*]. The river endmembers are calculated using Sal=0 and alkalinity values of 1181, 845, 788, 1707, and 1540 µmol/kg for the Ob, Yenisey, Lena, Yukon, and Mackenzie Rivers, respectively **[***Cooper et al., 2008*] multiplied with the partial distribution of these rivers to the total endmember [*Holmes et al, 2002*]. Gray arrows indicate sea-ice melting and sea-ice formation, relative to the Atlantic – Eurasian river water mixing line. Green ellipse includes the data points at ~50 m in the TPD (stations 309 – 333 and 349 – 352) and orange ellipse indicates the waters at ~50 m north of the TPD. Laptev Sea data points (stat. 407 and 411) are surrounded by a blue square and are consistent with mixing with river water and a strong sea-ice formation/ brine input signal in the deepest layer of stat. 411 (see text section 5.2).

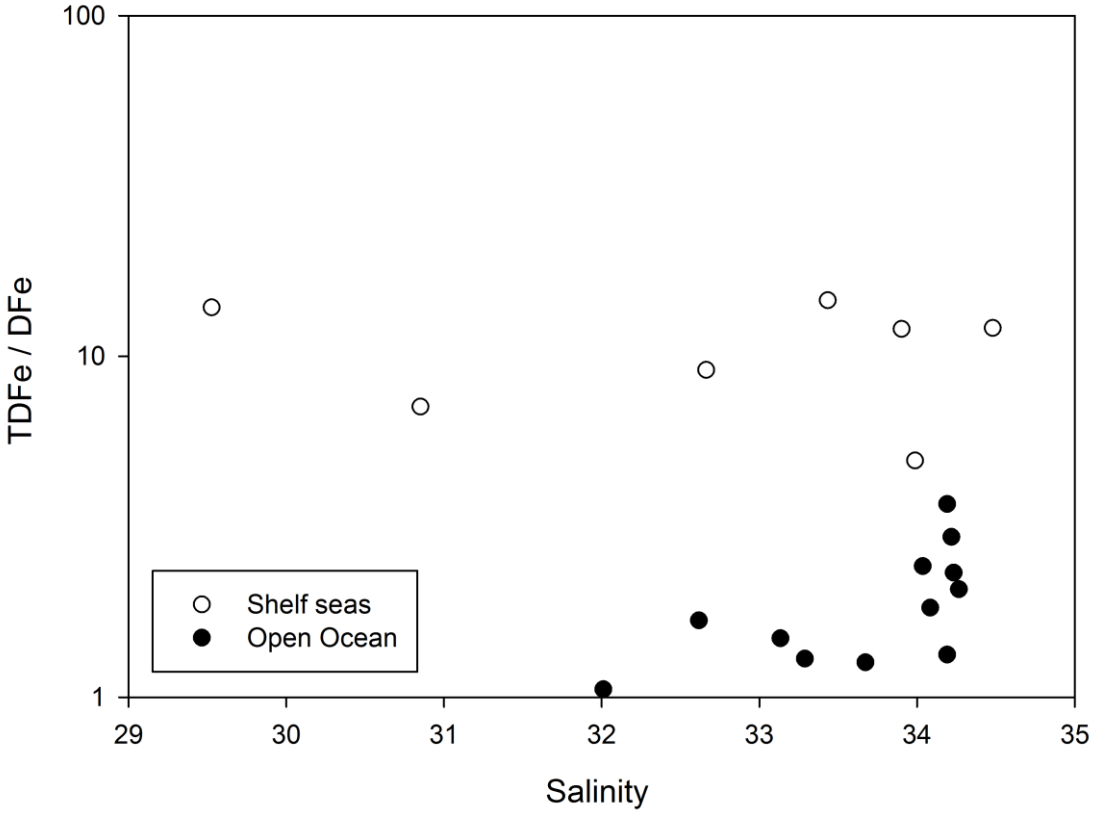

Fig. 11. Ratio total iron (TFe) over dissolved iron (DFe) for all points in the upper 100 m at shelf stations (open circles) and open ocean stations (closed circles). Shelf Sea Stations are indicated in Fig 1b.